AD-A093 038 EIC LABS INC NEWTON MA F/G 10/3
EXPLORATORY DEVELOPMENT OF AN ELECTRICALLY RECHARGEABLE LITHIUM--ETC(U)
OCT 80 K M ABRAHAM, J L GOLDMAN, M D DEMPSEY DAAK20-79-C-0267
UNCLASSIFIED DELET-TR-79-0267-F NL

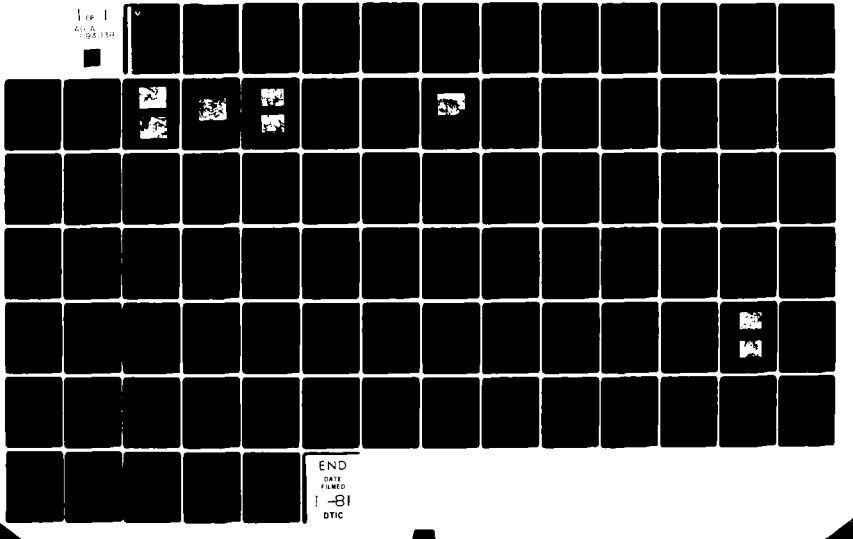

END
DATE FILMED
1-81
DTIC

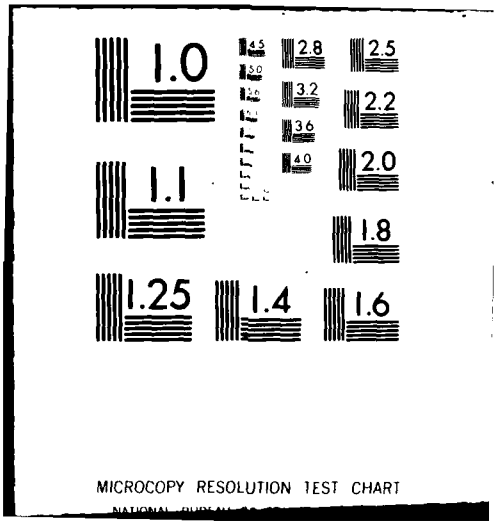
1.0
1.1
1.25
1.4
1.6
1.8
2.0
2.2
2.5
2.8
3.2
3.6
4.0
4.5
5.0
MICROCOPY RESOLUTION TEST CHART

Research and Development Technical Report
DELET-TR-79-0267-F

EXPLORATORY DEVELOPMENT OF AN ELECTRICALLY RECHARGEABLE LITHIUM BATTERY

K. M. Abraham
J. L. Goldman
M. D. Dempsey
G. L. Holleck

EIC Laboratories, Inc.
55 Chapel Street
Newton, MA 02158

October 1980

Final Report for Period 2 July 1979 - 1 July 1980

Prepared for:
ELECTRONICS TECHNOLOGY & DEVICES LABORATORY

ERADCOM

US ARMY ELECTRONICS RESEARCH AND DEVELOPMENT COMMAND
FORT MONMOUTH, NEW JERSEY 07703

NOTICES

Disclaimers

The citation of trade names and names of manufacturers in this report is not to be construed as official Government indorsement or approval of commercial products or services referenced herein.

Disposition

Destroy this report when it is no longer needed. Do not return it to the originator.

Unclassified

SECURITY CLASSIFICATION OF THIS PAGE (When Data Entered)

REPORT DOCUMENTATION PAGE

READ INSTRUCTIONS BEFORE COMPLETING FORM

1. REPORT NUMBER: DELET-TR-79-0267-F	2. GOVT ACCESSION NO.: AD-A093 038
3. RECIPIENT'S CATALOG NUMBER:	
4. TITLE (and Subtitle): Exploratory Development of an Electrically Rechargeable Lithium Battery,	5. TYPE OF REPORT & PERIOD COVERED: FINAL REPORT 7-2-79 to 7-1-80
	6. PERFORMING ORG. REPORT NUMBER:
7. AUTHOR(s): K.M./Abraham, J.L./Goldman, M.D./Dempsey, G.L./Holleck	8. CONTRACT OR GRANT NUMBER(s): DAAR20-79-C-0267
9. PERFORMING ORGANIZATION NAME AND ADDRESS: EIC Corporation 55 Chapel Street Newton, Massachusetts 02158	10. PROGRAM ELEMENT, PROJECT, TASK AREA & WORK UNIT NUMBERS: 1L162705AH94 11 771
11. CONTROLLING OFFICE NAME AND ADDRESS: US Army Elct Tech & Dvcs Laboratory ATTN: DELET-PR, Fort Monmouth, NJ 07703	12. REPORT DATE: October 1980
	13. NUMBER OF PAGES: 74
14. MONITORING AGENCY NAME & ADDRESS (If different from Controlling Office): Final rept. 2 Jul '79 - 1 Jul 80,	15. SECURITY CLASS. (of this report): Unclassified
	15a. DECLASSIFICATION/DOWNGRADING SCHEDULE:

16. DISTRIBUTION STATEMENT (of this Report)

Approved for Public Release;
Distribution Unlimited

17. DISTRIBUTION STATEMENT (of the abstract entered in Block 20, if different from Report)

18. SUPPLEMENTARY NOTES

19. KEY WORDS (Continue on reverse side if necessary and identify by block number)

Vanadium Oxides, Channel Structure, Discharge Characteristics, Rechargeability, Cycling Behavior, Hermetically Sealed Cells, Spirally Wound Cells, Prismatic Cells.

20. ABSTRACT (Continue on reverse side if necessary and identify by block number)

The cathodic behavior of V_6O_{13} was investigated in rechargeable Li cells of the type, Li/2Me-THF,LiAsF$_6$/V_6O_{13},C.

Two forms of V_6O_{13} were synthesized and characterized. These were a stoichiometric form, i.e., $VO_{2.17}$, and a slightly non-stoichiometric form, i.e., $VO_{2.19}$.

Stoichiometric V_6O_{13} was prepared by heating requisite quantities of V_2O_5 and

DD FORM 1 JAN 73 1473 EDITION OF 1 NOV 65 IS OBSOLETE

Unclassified

SECURITY CLASSIFICATION OF THIS PAGE (When Data Entered)

412102

JOB

(BLOCK 20)

V powder for 24 hrs. at 650°C. It was characterized by X-ray and SEM data. SEM analysis revealed this oxide to be a highly crystalline material composed of 4-5 um wide and 14-18 um long crystallites. For a cathode having a theoretical capacity density of 20 mAh/cm^2 (based on 1 e$^-$/V), the utilization in the early cycles was ~0.6 e$^-$/V at current densities of 0.5, 1.0 and 2.0 mA/cm^2 and 0.45 e$^-$/V at 4 mA/cm^2. Rate-capacity behavior similar to these was exhibited also by cathodes having capacity densities of 10 mAh and 30 mAh per cm^2. The discharge of 1.9V proceeded in four distinct voltage regions with a mid-discharge potential of ~2.3V. The cathode exhibited good rechargeability. One cell was cycled 80 times with a steady cathode utilization of 0.52 e$^-$.V,

The slightly non-stoichiometric V_6O_{13} was prepared by the thermal decomposition of NH_4VO_3 at 450°C. X-ray diffraction pattern of this material was virtually identical to that of stoichiometric V_6O_{13}. However, SEM data revealed it to be composed of much smaller particles with very little apparent crystallinity. First discharge of the material resulted in a higher capacity than the stoichiometric oxide. For example, capacities between 0.90 and 1.0 e$^-$/V were obtained at current densities between 0.50 and 2.0 mA/cm^2. The extra capacity results in a plateau at ~2.1V. In the first charge, a loss in capacity amounting to 15-20% of the first discharge occurs. This loss is independent of charge current densities between 0.1 and 2.0 mA/cm^2. With continued cycling, a gradual loss in cathode utilization occurs in the early cycles. After 15 cyles or so, the cathode utilization becomes steady at ~0.60 e$^-$/V.

The discharge characteristics of the stoichiometric oxide at 60°C were similar to that of non-stoichiometric oxide at room temperature.

The rechargeability of both the oxides were found to be sensitive to the lower voltage cutoff. The safest limits of cycling were 3.0 and 1.9V. Potentiostatic discharges of the oxides between 1.9 and 1.3V revealed a high capacity irreversible reduction process at about ~1.6V.

Three types of hermetically sealed cells were constructed and tested. In a high capacity (5Ah) prismatic cell utilizing the non-stoichiometric oxide, energy densities of 106 Whr/kg and 190 Whr/DM^3 were achieved.

TABLE OF CONTENTS

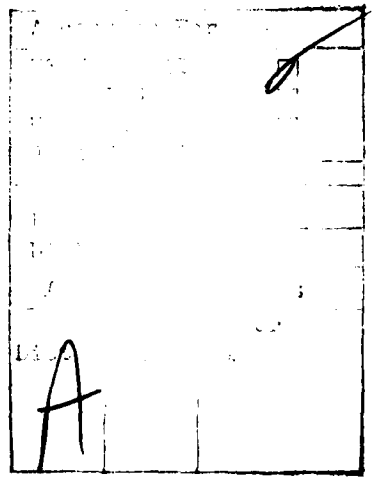

LIST OF ILLUSTRATIONS

LIST OF ILLUSTRATIONS
(continued)

LIST OF ILLUSTRATIONS
(continued)

LIST OF TABLES

1. INTRODUCTION

Lithium secondary battery technology has been actively pursued for more than 20 years (1). Some striking advances have been made in the past ten years. These have been made possible by the discoveries (2) of new organic solvent/Li salt systems in which the Li electrode can be recharged with high efficiency. Especially note-worthy are the EIC System (3), 2Me-THF/$LiAsF_6$ and the Exxon electrolyte (4), 1,3-dioxolane/$LiClO_4$. Unfortunately, the 1,3-dioxolane/$LiClO_4$ system shows a tendency to detonate upon impact and therefore has been abandoned. Recently, we have demonstrated 100-200 deep discharge cycles in Li/TiS_2 cells utilizing 2Me-THF/$LiAsF_6$ electrolyte (5). The Li electrode in these cells exhibited an average cycling efficiency of 96%.

The status of the rechargeable positive electrodes was recently reviewed by Abraham (6). During the past two decades a large variety of materials have been discovered and evaluated. The degree of understanding of these materials, however, varies considerably. The most extensively studied and promising materials are solid state cathodes which undergo intercalation or topochemical reactions with Li (6).

An ideal intercalation reaction involves the interstitial introduction of a guest species into a host lattice without structural modification of the host. Such a reaction is reversible because similar transition states are readily achieved for both the forward and reverse reactions, leading to close compliance with the thermodynamic principle of microscopic reversibility. In an actual intercalation reaction, the bonding within the host lattice may be slightly perturbed (e.g., a slight expansion of the host lattice may occur). The inherent reversibility of intercalation suggests its utility as a mechanism for reversible electrode reactions (Eqn. 1).

$$xLi^+ + xe^- + MY_n \rightleftharpoons Li_xMY_n \qquad (1)$$

Similar reactions which depend on the structure of the host but resulting in somewhat larger structural modifications, such as cleavage of certain bonds, are termed topotactic or topochemical. These reactions may be either reversible or irreversible depending upon the specific nature of the structural changes. Classes of materials which undergo topochemical or intercalation Li reaction are: transition metal sulfides, selenides or oxides with layered structures and transition metal sulfides or oxides with three dimensional network structures. Of all these materials only TiS_2 received any significant developmental effort. The excellent reversibility and chemical compatibility of TiS_2 in practical Li cells have been demonstrated recently at EIC (5). Despite its impressive performance characteristics, TiS_2 does not have the energy density required for many potential applications of secondary Li cells. Therefore, any new material with improved characteristics is a welcome addition.

A potentially attractive group of materials are the transition metal oxides. Preliminary studies of several rutile and perowskite related oxides have been carried out recently by Murphy and coworkers (7). These studies have indicated that several vanadium oxides, particularly V_6O_{13}, are potentially attractive materials as high energy cathodes for Li cells.

The vanadium oxides, V_2O_5, V_6O_{13} and VO_2 (B) comprise a class of framework compounds consisting of shear structures derived from the ReO_3 lattice (6). The parent structure contains an extended network of channels intersecting in three mutually perpendicular directions. These channels may be visualized as a rising from the sharing of square faces of individual, vacant cavities (Figure 1).

An idealized V_2O_5 structure may be derived from an ReO_3 lattice by removing oxygens from every second (200) plane and closing the structure along the shear vector $\frac{1}{2}[100]$. The resulting shear structure consists of distorted VO_6 octahedra joined by edge sharing among themselves along [001] into single zig-zag chains linked together by corner sharing to form single sheets. These sheets are joined by means of additional corner sharing into a three-dimensional lattice. The resulting structure contains asymmetric V=O---V units.

The V_6O_{13} lattice may be regarded as a shear structure of V_2O_5. This structure contains distorted VO_6 octahedra joined by extensive edge sharing into both single and double zig-zag chains running parallel to (010). Both the single and double chains are linked by additional edge sharing into single and double sheets, respectively, both lying parallel to the (100) plane. The sheets are interleaved and joined together by corner sharing to form a three-dimensional lattice. This structure contains tricapped cavities joined through shared square faces. The asymmetric V=O---V linkages are absent in the structure.

The metastable VO_2 (B), has a structure related to those of V_2O_5 and V_6O_{13}. The structure may be visualized simply as that obtained by removing the sheets of single chains from the V_6O_{13} structure.

In this report we present the results of a detailed study of the performance characteristics of V_6O_{13} in secondary Li cells with 2Me-THF/$LiAsF_6$ electrolyte. The major areas of investigation were: synthesis and characterization of V_6O_{13}; evaluation of rechargeability of V_6O_{13} with identification of major capacity limiting factors and construction and testing of hermetically sealed cells.

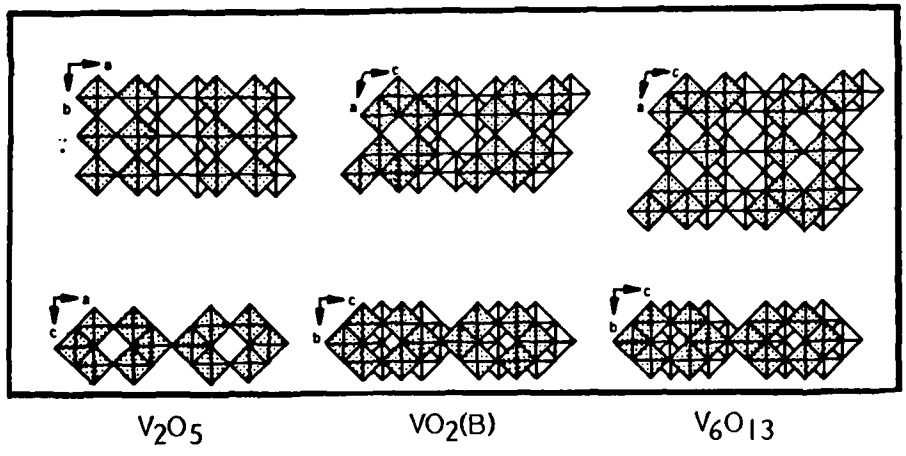

Fig. 1. Corresponding views of V_2O_5, V_6O_{13}, and $VO_2(B)$ constructed from idealized MO_6 octahedra (Ref. 6).

2. SYNTHESIS AND CHARACTERIZATION OF V_6O_{13}

V_6O_{13} was prepared according to two different procedures: (i) by heating of stoichiometric amounts of V and V_2O_5 in a sealed, evacuated quartz tube at 650°C (Eqn. 2)

$$13\ V_2O_5 + 4V \xrightarrow{650°C} 5\ V_6O_{13} \qquad (2)$$

The material prepared by this method is stoichiometric V_6O_{13}, i.e., $VO_{2.17}$ (ii) by the thermal decomposition of NH_4VO_3 in an inert atmosphere at 450°C. The V_6O_{13} obtained under carefully controlled conditions is slightly non-stoichiometric, i.e., $VO_{2.19}$.

2.1 Stoichiometric V_6O_{13}

In a typical preparation, an intimate mixture consisting of 11.82g (65 mmoles) of V_2O_5 (Alfa-Ventron) and 1.02g (20 mmoles) of V powder (Alfa-Ventron, -325 mesh) was heated in an evacuated, sealed, quartz tube at 650°C. Samples were prepared using heating times of 8 hr, 16 hr and 24 hr. X-ray powder patterns of the materials are tabulated in Table 1. Scanning electric micrographs (SEM) of the materials are depicted in Figures 2A through 2E.

All the samples were composed of well-shaped crystals, although their average sizes varied from sample to sample. In the sample heated for 8 hr (Fig. 2A), the crystals were 15-40 μm long and 3-6 μm wide; in the sample heated for 16 hr (Fig. 2B), they were 15-30 μm and 3-6 μm wide. In one of the samples heated for 24 hr (Fig. 2C), the crystals were 14-18 μm long and 4-5 μm wide. In a second 24 hr heated sample, Figures 2D and 2E), the crystals were 10-40 μm long and 5-10 μm wide. The X-ray patterns of all the three samples were essentially identical. However, the relative intensities of the lines at 3.52Å and 3.32Å showed a systematic variation with heating time. The relative intensities in the pattern of the 24 hr sample were very close to those reported by Wilhelmi, et al. (9). As would be seen later, the 24 hr sample exhibited the best electrochemical performance.

2.2 Non-Stoichoimetric V_6O_{13}

In a typical preparation, 17.33g NH_4VO_3 contained in a graphite boat was heated in a flowing argon atmosphere (flow rate, 450 cc/min) at the following temperature ranges. Initially, the temperature was raised from 25°C to 400°C in about 1/2 hr. The temperature was then increased to 450°C and kept at this temperature for another 2 hrs. Finally, the material was annealed at 550°C for 1 hr. The dark product weighed 12.73g. The composition of the oxide was calculated to be $VO_{2.19}$. Its X-ray pattern, obtained by the Debye-Sherer technique is shown in Table 2. The pattern is very much similar to

Table 1

X-Ray* Data for Vanadium Oxides

Oxide	2θ<, Degrees	d, Å	Relative Intensity
V_6O_{13} from V_2O_5 and V; heating time of 8 hr at 650°C	25.2	3.53	40
	26.8	3.32	100
	30.1	2.97	40
	33.4	2.68	45
	36.0	2.49	5
	45.4	2.00	80
	49.2	1.85	30
	53.9	1.70	5
	55.1	1.67	5
	57.1	1.61	5
	59.7	1.55	5
V_6O_{13} from V_2O_5 and V; heating time of 16 hr at 650°C	25.4	3.50	70
	26.9	3.31	100
	30.2	2.96	35
	33.5	2.57	25
	36.1	2.49	5
	45.6	1.99	80
	49.6	1.84	30
	54.1	1.69	5
	55.3	1.66	5
	57.2	1.61	5
	59.9	1.54	5
V_6O_{13} from V_2O_5 and V; heating time of 24 hr at 650°C	25.3	3.52	75
	26.8	3.32	85
	30.0	2.98	30
	33.4	2.68	35
	36.0	2.47	5
	45.5	1.99	100
	49.4	1.84	30
	54.0	1.70	5
	55.2	1.66	5
	57.1	1.61	5
	59.7	1.55	5

*CuK_α radiation, $\lambda = 1.5405$ Å; Debye-Scherrer technique.

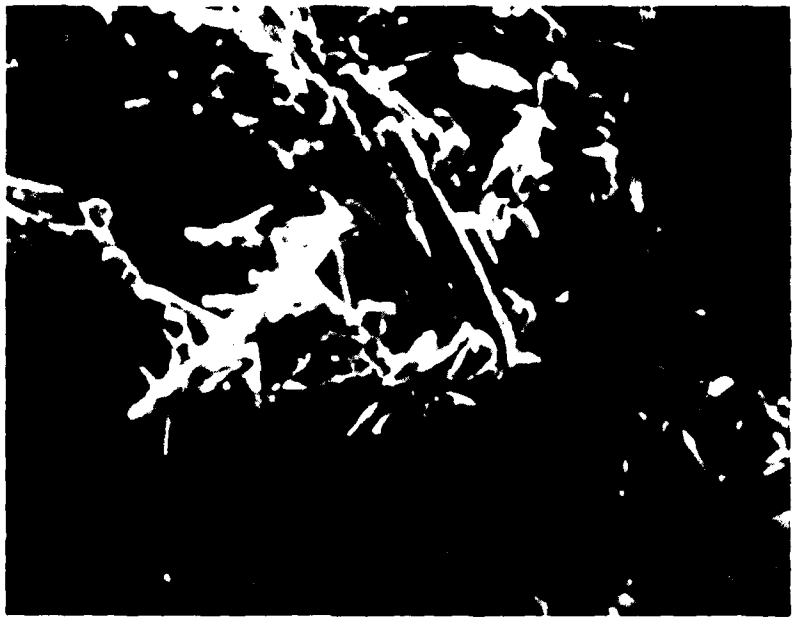

Fig. 2A. SEM photograph of stoichiometric V_6O_{13} prepared using a heating time of 8 hours. Magnification, 1000X.

Fig. 2B. SEM photograph of stoichiometric V_6O_{13} prepared using a heating time of 16 hours. Magnification, 1000X.

Fig. 2C. SEM photograph of stoichiometric V_6O_{13} prepared using a heating time of 24 hours. Magnification, 1000X.

Fig. 2D. SEM photograph of a second sample of V_6O_{13} prepared using a heating time of 24 hours. Magnification, 1000X.

Fig. 2E. SEM of the sample in Fig. 1D at 2000X.

Table 2

X-Ray Data* for V_6O_{13} Prepared from NH_4VO_3

2θ<, degrees	d, Å	Relative Intensity
15.25	5.81	W
17.95	4.94	W
25.55	3.49	S
27.15	3.28	S
30.70	2.91	M
33.75	2.66	M
36.35	2.47	W
45.80	1.98	S
49.95	1.83	S
53.95	1.70	M
57.40	1.61	M
60.10	1.54	M
52.10	1.49	W
66.65	1.40	W
69.9	1.35	M

*Debye-Sherer technique; Cu K_α Radiation, λ = 1.5418 Å.

that of the stoichiometric oxide. An SEM of the material is shown in Fig. 3. The non-stoichiometric oxide is apparently composed of much smaller crystals, although the present SEM does not show any crystalline nature. Note that the X-ray data indeed suggest that the material is crystalline.

In optimizing the synthesis, it was found that a very careful control of the Ar flow rate is of utmost importance in obtaining the desired product in a pure form. The argon flow rate controls the residence time of the liberated NH_3, the reducing agent which determines the V to oxygen ratio in the product. In different preparations with argon flow rates lower than 450 cc/min*, we have synthesized oxides of compositions, $VO_{1.88}$, VO_2, $VO_{2.04}$ and $VO_{2.08}$. X-ray patterns of $VO_{2.04}$ and VO_2 are given in Table 3. All these lower oxides exhibited electrochemical characteristics much inferior to that of $VO_{2.19}$ (see later).

2.3 Heat Treatment of Non-Stoichiometric V_6O_{13}

The effect of heat treatment on the non-stoichiometric V_6O_{13} was evaluated by heating a sample of the oxide in a sealed, evacuated quartz tube for 16 hr at 650°C. Although the X-ray pattern did not show any significant change, SEM data revealed that the material had been converted to a more crystalline form with average crystals of 20-30 μm long and 3-5 μm wide. The discharge of this material resembled the stoichiometric oxide (see later).

2.4 Chemical Lithiation of Non-Stoichiometric V_6O_{13}

Lithium capacity of non-stoichiometric V_6O_{13}, was determined by chemical lithiation with n-BuLi according to reaction 3.

$$x\text{n-BuLi} + V_6O_{13} \longrightarrow Li_xV_6O_{13} + \frac{x}{2}\ \text{Octane} \qquad (3)$$

In a reaction, 1.46g (2.84 mmoles) of V_6O_{13} was stirred at room temperature with a large excess (34.2 mmoles) of 0.2N n-BuLi in hexane for 24 hr. The solution was filtered and the amount of unreacted n-BuLi was determined by titration with 0.1N HCl. The amount of n-BuLi reacted with V_6O_{13} was found to be 22.1 mmoles which was equivalent to an uptake of 7.78 mmoles of Li/mole of V_6O_{13}.

In order to examine the chemical reversibility of the Li in $Li_{7.8}V_6O_{13}$, the latter was treated with an excess of CH_3CN/I_2 solution and the amount of I_2 consumed according to reaction was determined by titrating

*The flow rate required to obtain $VO_{2.19}$ may vary with sample size and the container tube size.

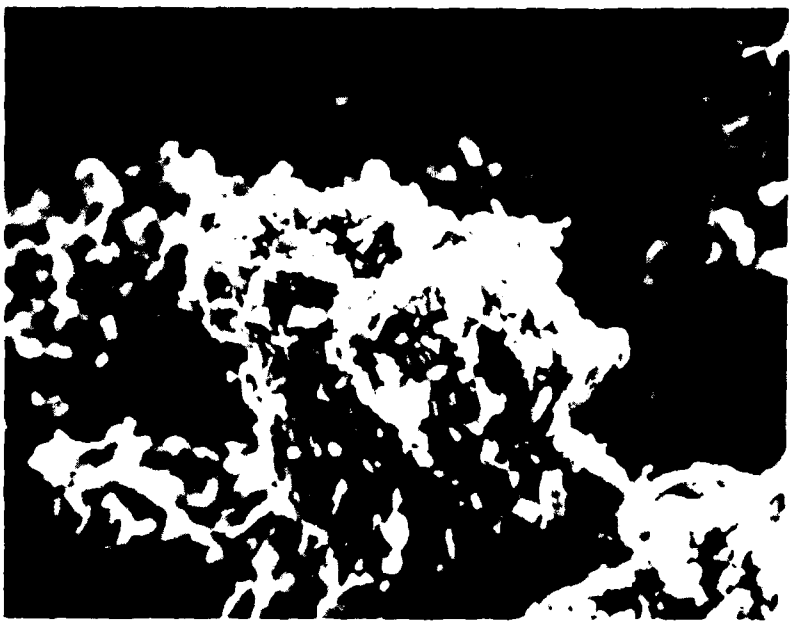

Fig. 3. SEM photograph of non-stoichiometric V_6O_{13}. Magnification, 1000X.

Table 3

X-Ray Data for Lower V-Oxides from NH_4VO_3

Oxide	2θ, degrees	d, Å	Relative Intensity
VO_2	23.0	3.87	0.3
	25.5	3.49	1.0
	29.5	3.03	0.4
	30.5	2.93	0.4
	34.0	2.64	0.6
	44.3	2.05	0.6
	45.0	2.01	0.6
	49.5	1.84	0.7
$VO_{2.04}$	14.3	6.22	0.4
	15.3	5.81	0.4
	20.5	4.33	0.5
	25.5	3.50	1.0
	29.0	3.07	0.5
	30.3	2.95	0.5
	33.8	2.65	0.6
	44.3	2.05	0.5
	45.3	2.00	0.50
	49.7	1.83	0.7
	59.3	1.56	0.5

the unreacted I_2 with standard $Na_2S_2O_3$ solution.

$$Li_xV_6O_{13} + \frac{x}{2} I_2 \longrightarrow xLiI + V_6O_{13} \qquad (4)$$

It was found that only 5 Li could be removed by reaction 4. However, an examination of the potentials of the redox couples, I_2/I^- (2.8V) and $Li_xV_6O_{13}/V_6O_{13}$ (2.8V-2.2V) indicates that reaction 4 may lead to an equilibrium situation. It appears that an oxidizing agent more powerful than I_2 would be necessary to completely deintercalate $Li_{7.8}V_6O_{13}$. The X-ray pattern of $Li_{7.8}V_6O_{13}$ is shown in Table 4.

Reaction of stoichiometric V_6O_{13} results in an uptake of only 4Li per V_6O_{13} (6,7).

Table 4

X-Ray Data of $Li_{7.8}V_6O_{13}$

2θ, degrees	d, Å	Relative Intensity
15.1	5.86	0.5
17.9	4.95	0.5
21.6	4.12	0.4
24.2	3.68	1.0
27.2	3.28	0.8
30.4	2.94	0.5
44.3	2.04	0.3
45.6	1.99	0.6
47.0	1.93	0.6
54.3	1.69	0.4

3. ELECTROCHEMICAL EVALUATION OF VANADIUM OXIDES

3.1 General Experimental

Cathodic behavior of vanadium oxides were evaluated in cells of the type,

$$Li/2Me\text{-}THF,LiAsF_6/V_6O_{13},C$$

The system, 2Me-THF,$LiAsF_6$ as the electrolyte of choice for secondary Li cells has recently been demonstrated (3, 5).

3.1.1 Preparation of Electrolyte

2-methyl tetrahydrofuran, obtained from Aldrich Chemical Co., was distilled over CaH_2 on a spinning band fractionating column (Perkin-Elmer 251) in a nitrogen atmosphere at a 5:1 reflux ratio. The middle 70% fraction was collected. A 1.5M $LiAsF_6$ electrolyte was prepared by adding an appropriate amount of $LiAsF_6$ (U.S. Steel Agri-Chemicals, electrochemical grade) to cooled (<0°C) 2Me-THF. The cooling is necessary to minimize possible decomposition (10). The electrolyte was further purified by the APA procedure (10). Typically, the electrolyte prepared in this manner exhibited thin plate (1 coul/cm^2)Li recycling efficiencies of 95-96%.

3.1.2 Cathode Preparation

The cathodes were prepared as pressed powder electrodes. An intimate mixture of V oxide, carbon (Shawinigan 50% compressed or AGM graphite and 10 w/o Teflon was prepared in a blender. The ratio of V to carbon was varied in the optimization studies. The optimized cathodes contained 70 w/o V_6O_{13}, 20 w/o carbon and 10 w/o Teflon. The mixture was pressed on either side of an expanded Ni screen (Exmet Corporation 5 Ni7-4/o) at a pressure of ~2000 lbs/in^2. The electrodes typically had a thickness of 0.6-0.8 mm.

3.1.3 Test Cells

Most of the experiments were carried out in a prismatic glass cell, shown schematically in Fig. 4. In these cells, the electrode package comprised one cathode flanked on either side by a Li electrode wrapped in 1 ml thick Celgard 2400 (Celanese Corporation) separator. The Li electrode was fabricated from a 15 mil thick Li foil obtained from Foote Mineral Company and pressing the foil on one side of an expanded Ni screen. Each electrode had an area of 8 cm^2 (3.2 cm x 2.5 cm). The cell was completed with an appropriate amount of 2Me-THF/1.5 $LiAsF_6$.

PRISMATIC TEST CELL

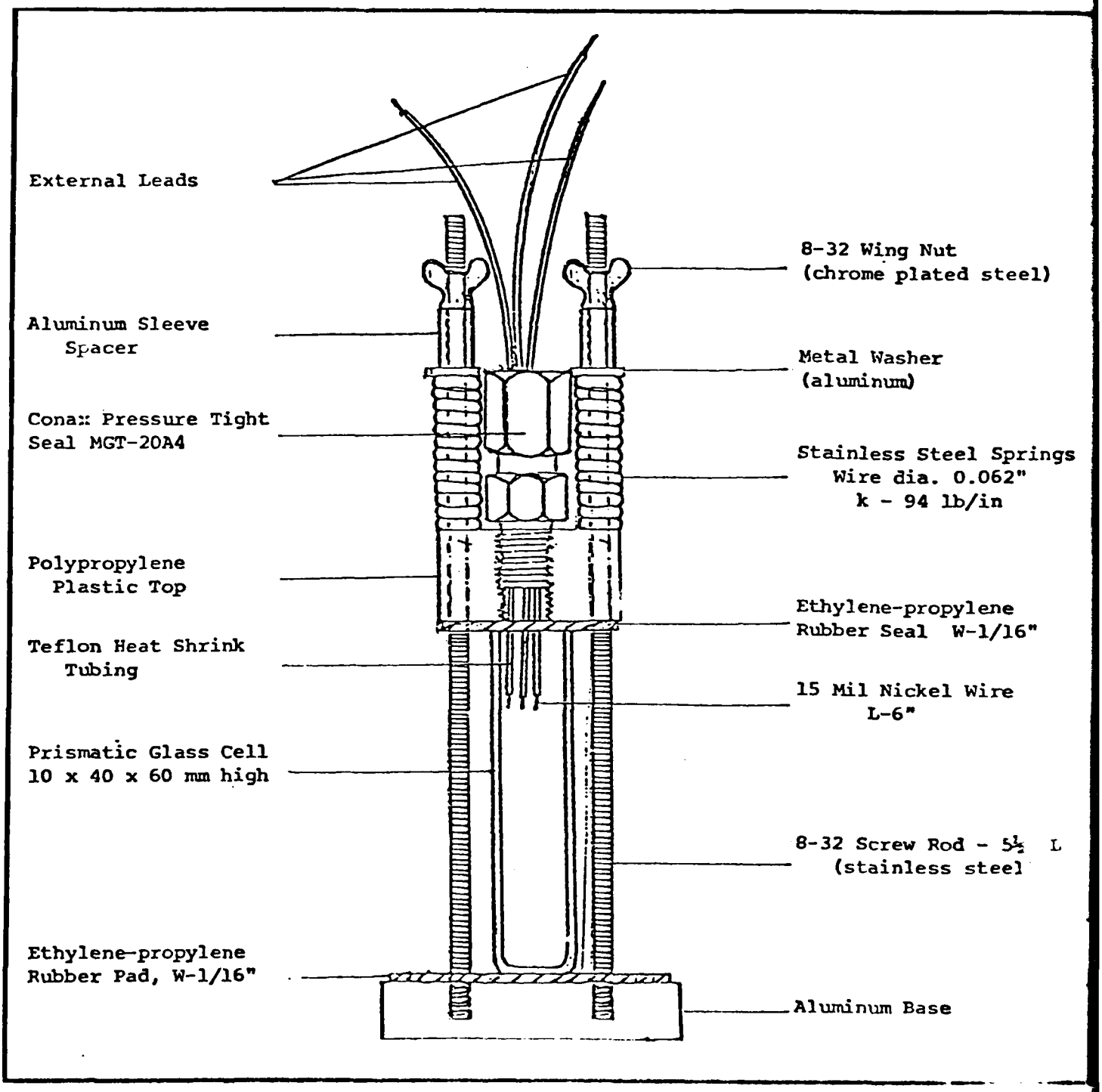

Fig. 4. Schematic of laboratory test cell.

Tests were also carried out in hermetically sealed laboratory cells, hermetically sealed spirally wound cells and in hermetically sealed, high capacity prismatic cells. Specifications of these cells will be discussed later.

3.2 Cathodic Behavior of Vanadium Oxides

3.2.1 Discharge Characteristics of NH_4VO_3 Decomposition Products

It was noted earlier that from the thermal decomposition of NH_4VO_3, in addition to V_6O_{13}, i.e., $VO_{2.19}$, a series of lower oxides can be prepared depending upon the reaction conditions. The lower oxides synthesized in several preparations were $VO_{1.88}$, VO_2, $VO_{2.04}$ and $VO_{2.08}$. Discharge characteristics of all of these oxides were evaluated. The primary discharges of the oxides, $VO_{1.88}$, VO_2, $VO_{2.04}$, $VO_{2.08}$ and $VO_{2.19}$, obtained galvanostatically at 8 mA (0.5 mA/cm^2) are shown in Fig. 5. The discharge data are summarized in Table 5. The data indicate that the cathode capacities and the potentials at which the discharge proceed depend on the composition of the oxide. Thus for $VO_{1.88}$, although the discharge begins at $\sim$2.8V, the cell polarizes rapidly to $\sim$1.8V at which potential most of the discharge proceeded. For VO_2 and $VO_{2.04}$, the discharge curves show a plateau at $\sim$2.45V. The discharge curve for $VO_{2.08}$ shows two plateaus at $\sim$2.45V and $\sim$2.05V. The discharge curve for $VO_{2.19}$ shows a plateau at $\sim$2.75V, two downward sloping potential regions at $\sim$2.5 and 2.3V and another plateau at 2.1V. The potential profiles observed for $VO_{2.19}$ are identical to those found by Murphy (8) for V_6O_{13} prepared from NH_4VO_3. The latter exhibited a capacity of 1.1 e^-/V to a cutoff of 1.7V.

It is instructive to note here that in the first discharge of V_2O_5, about 20% of the capacity is observed at potentials above 3.0V (12). Therefore, the primary discharge characteristics of the oxides are useful in evaluating material purity.

3.2.2 Cycling Behavior of $VO_{2.19}$; The Non-Stoichiometric V_6O_{13}

Figure 6 shows the first two cycles of the non-stoichiometric V_6O_{13}. The discharge proceeds in discrete potential steps indicating phase transitions with the degree of Li incorporation. The discharge shows a fairly sharp cutoff to 1.9V with a capacity of $\sim$1.0 e^-/V the first discharge. (Additional irreversible capacity is obtained at lower potentials; see later.) In the first charge typically only 80-85% of this capacity is recharged. The capacity in the second cycle is nearly 100% of that in the first charge.

The potential plateaus in the first discharge occur at the approximate Li compositions in $Li_xV_6O_{13}$ of, $0<x\leq0.95$, $0.95<x\leq2.75$, $2.75<x\leq3.65$ and $3.65<x\leq6.05$. The three dimensional structure of V_6O_{13}

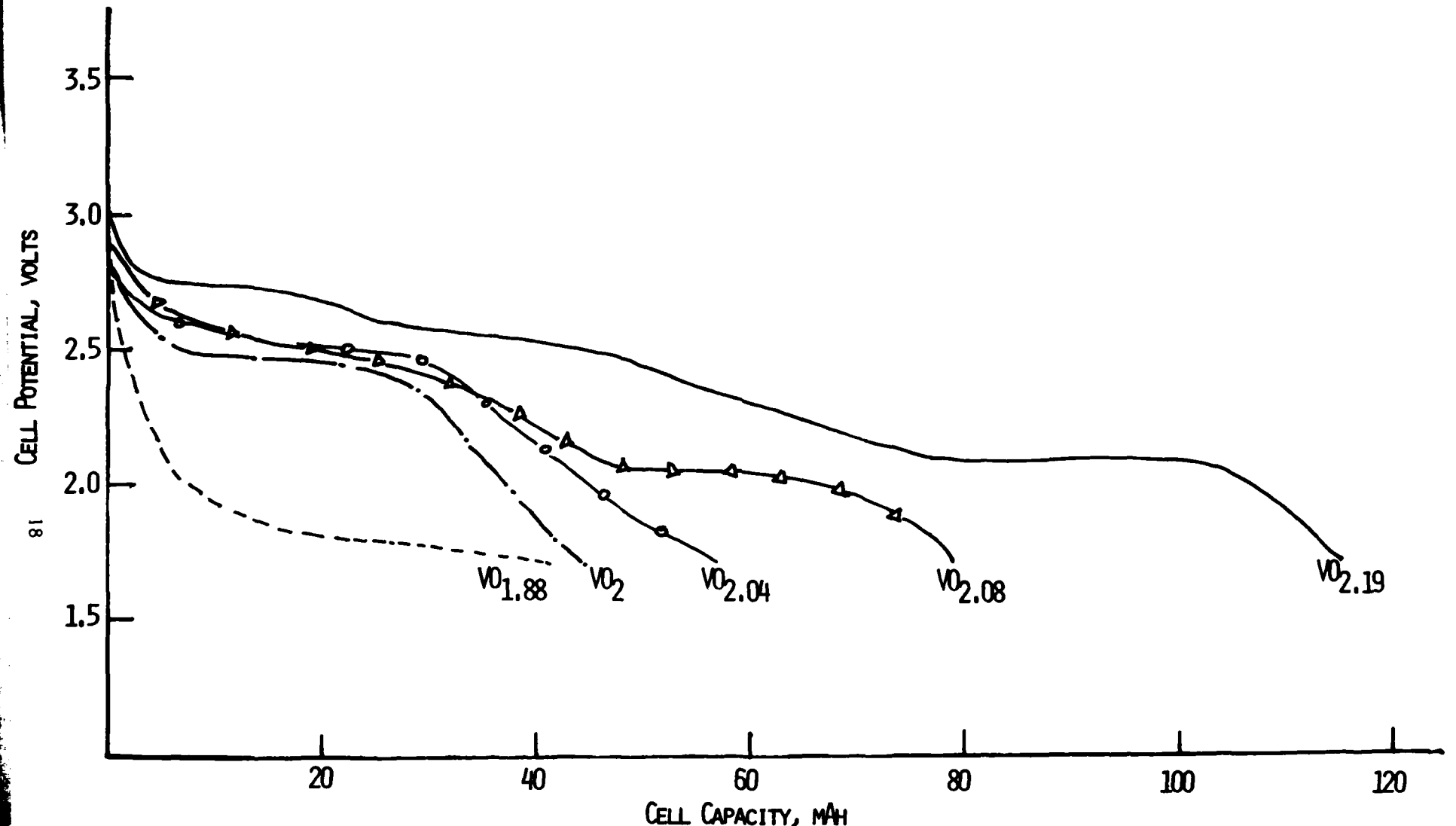

Fig. 5. Galvanostatic discharge curves for the various vanadium oxides synthesized by the thermal decomposition of NH_4VO_3. Current = 8 mA (0.5 mA/cm^2).

Table 5

Discharge Data for Vanadium Oxides

Current = 8 mA (0.5 mA/cm^2)

Cell No.	Oxide in the Cathode			Capacity* mAh	e^-/V
	Composition	gm	mmoles		
31	$VO_{1.88}$	0.31	3.82	32	0.31
24	VO_2	0.25	3.01	40	0.5
22	$VO_{2.04}$	0.32	3.83	60	0.58
35	$VO_{2.08}$	0.27	3.20	77	0.89
39	$VO_{2.19}$	0.31	3.80	112	1.10

*Capacity to 1.7V.

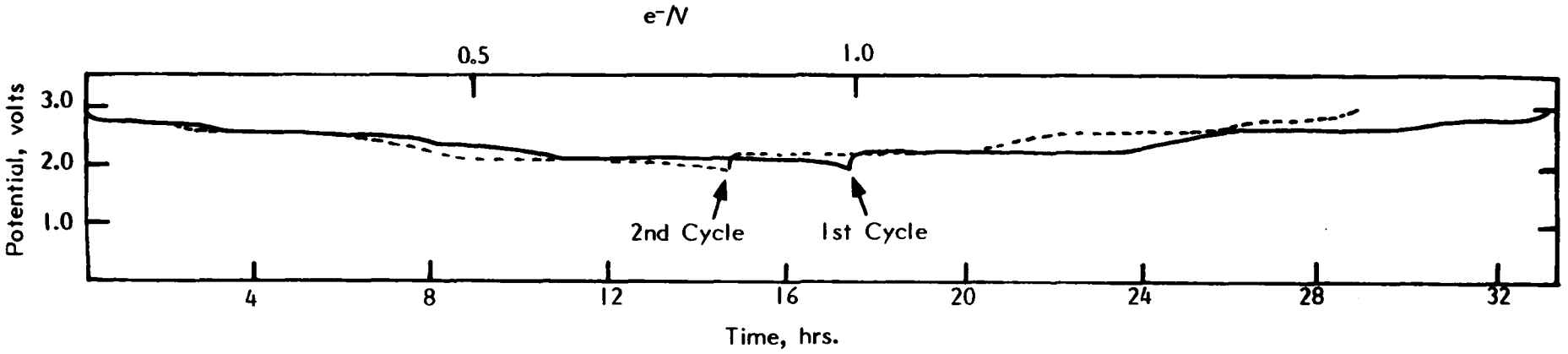

Fig. 6. The first two cycles of the non-stoichiometric oxide. Current density = 0.5 mA/cm^2.

contains 2 perowskite cavities (7). Each cavity contains 15 distorted square pyramidal sites which belong to two groups of 3 and 12 identical ones. In the first discharge, a capacity of nearly $4Li/V_6O_{13}$ is found at potentials >2.1V. This may involve the occupation of 2Li per cavity. Of the additional two lithiums discharging at ∿2.1V, one may be incorporated per cavity. It should be noted that with nBuLi, nearly 8Li can be incorporated into V_6O_{13} suggesting that the maximum Li capacity in non-stoichiometric V_6O_{13} is 4Li per cavity.

In the first charge about 15-20% of the capacity involved in the first discharge is not recharged. This capacity loss was independent of the current densities between 0.10 and 2.0 $mA.cm^2$. This fraction appears to be mostly the capacity involved in the higher voltage regions - primarily from the 2nd and 3rd phase regions. With continued cycling, the relative ratios of the capacities involved in the various phase regions of 2nd discharge seem to be maintained.

3.2.3 Cycling Behavior of V_2O_5 + V Products - The Stoichiometric V_6O_{13}

The first two cycles of a cell utilizing the stoichiometric oxide is shown in Fig. 7. This oxide sample was prepared using a heating time of 24 hr. The discharge proceeds in three distinct voltage steps corresponding to a capacity of 0.55 e^-/V. The end of discharge is indicated by a very small plateau at ∿2.0V and then a clear potential drop to 1.9V. In the present cell the three upper plateaus occur at the approximate Li compositions in $Li_xV_6O_{13}$ ternary of $0<x\leq0.75$, $0.75<x\leq1.5$ and $1.5<x\leq3.0$. Practically 100% rechargeablilty is observed in the first charge. The cathode exhibits excellent utilization at this value with continued cycling.

The significant difference between the non-stoichiometric and stoichiometric oxides at ambient temperature is the absence of the plateau in the latter at ∿2.1V. Consequently, the stoichiometric oxide exhibits 0.33 e^-/V less capacity then the non-stoichiometric oxide. The maximum capacity of the stoichiometric oxide determined by the nBuLi reaction is $4\ Li/V_6O_{13}$ or 0.66 e^-/V (7). This corresponds to the incorporation of 2Li per cavity in the oxide lattice.

The maximum capacity of 4Li per stoichiometric V_6O_{13} at ambient temperature appears to be determined by kinetic factors. This is indicated by the fact that by discharging the cell at 60°C, Fig. 8, an additional capacity of 0.33 Li/V is obtained with the extra capacity appearing at ∿2.1V as in the non-stoichiometric oxide. At 60°, the recharge was only 85% of the discharge, i.e., 0.72 e^-/V. When the cell was returned to room temperature, its behavior resembled that prior to the cycle at 60°C. It appears that in the non-stoichiometric oxide, the defect created by the extra oxygens reduces the activation energy for incorporation of >4Li per V_6O_{13}.

We have also evaluated the electrochemical performance of the V_2O_5 + V reaction products prepared using heating times of 8 hr and 16 hr. Although the potential profiles of cell cycles were identical to those of

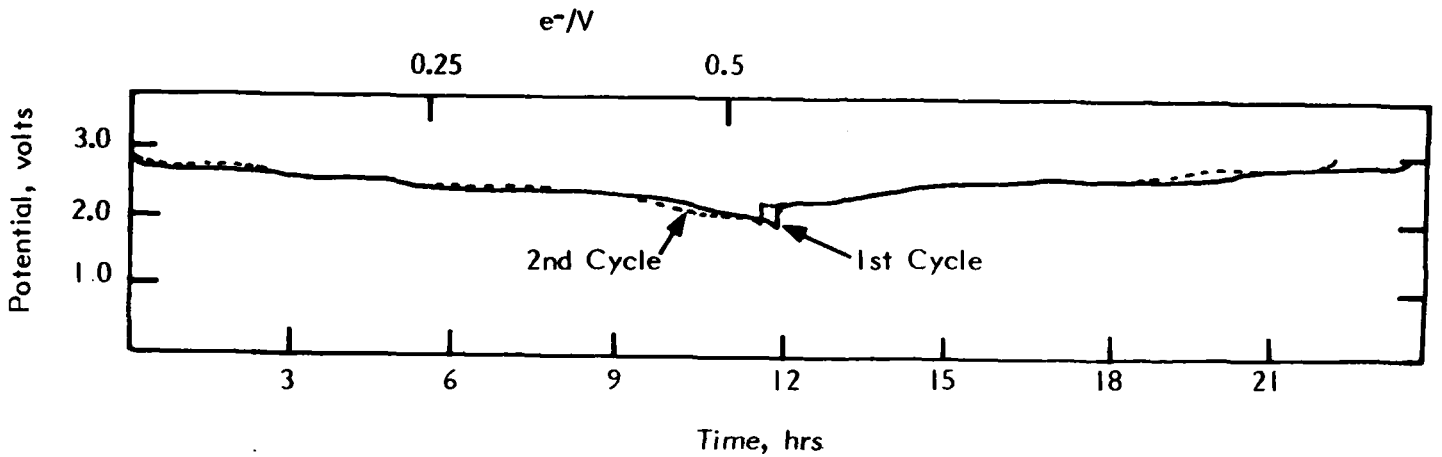

Fig. 7. The first two cycles of the stoichiometric oxide. Current density = 0.5 mA/cm^2.

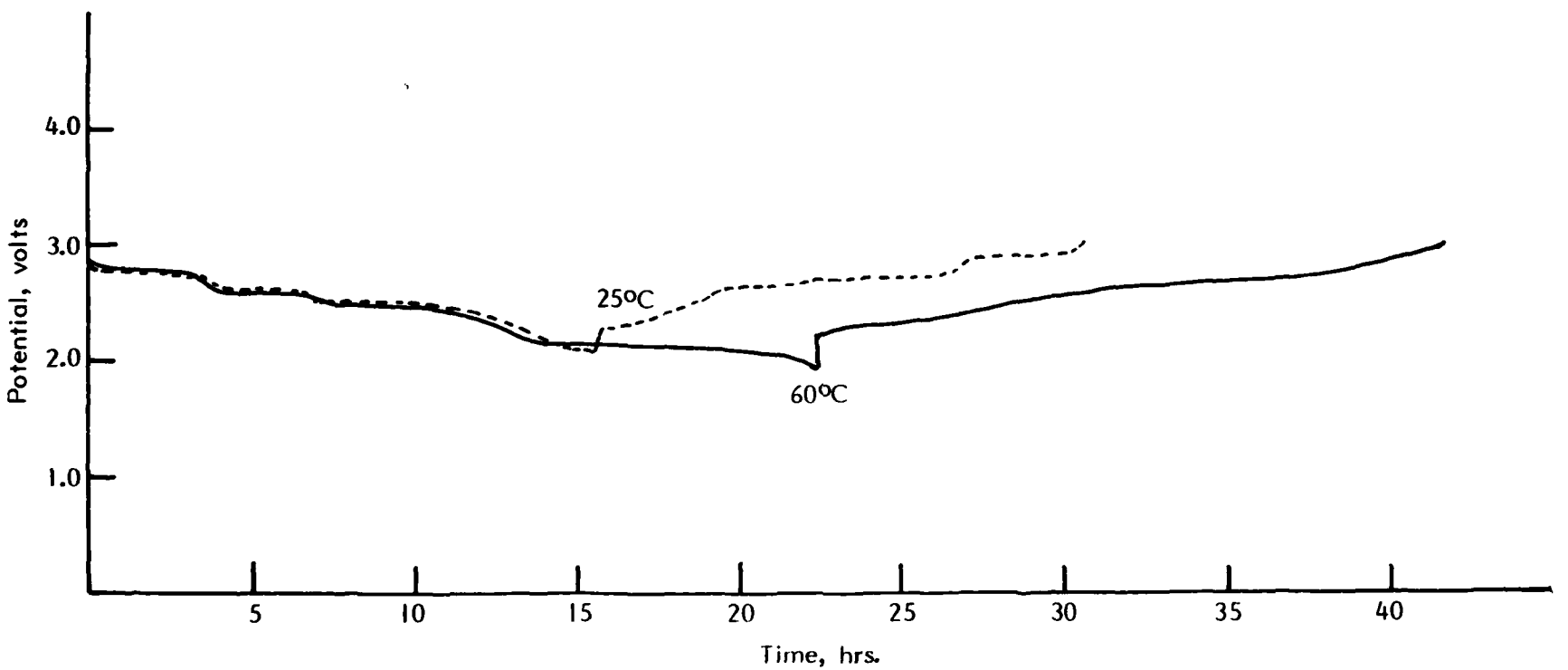

Fig. 8. Effect of temperature on the cycling of stoichiometric V_6O_{13}. Current density = 0.5 mA/cm^2. The 25°C cycle was the first cycle. The 60°C cycle was obtained after 12 cycles at 25°C.

the 24 hr sample shown in Fig. 7, the 8 hr and the 16 hr samples exhibited poorer cathode utilizations.

Therefore, all further studies of the stoichiometric oxide were carried out with samples prepared using a heating time of 24 hr.

3.2.4 Cycling Behavior of Heat-Treated $VO_{2.19}$

The SEM of a sample of non-stoichiometric V_6O_{13} heated for 16 hr at 650°C showed that the heat-treatment induces a higher degree of crystallinity. After the heat treatment, the appearance of the crystals was similar to that of the stoichiometric oxide. The potentials profiles of the discharge/charge curves of a cell utilizing this material were identical to those of a stoichiometric oxide cell. However, in the one sample tested the cathode utilization corresponded to only 0.4 e^-/V.

It appears that heat-treatment of $VO_{2.19}$ results in the removal of the extra oxygens responsible for its defect structure and converts it to the stoichiometric oxide.

3.3 Evaluation of Factors Limiting Rechargeability of V_6O_{13}

3.3.1 Effect of Carbon

Two cells, one utilizing the stoichiometric V_6O_{13} and the other the non-stoichiometric V_6O_{13}, were evaluated. The cathodes in these cells contained 90% V_6O_{13} and 10 w/o Teflon. Each cell, with one pressed cathode had an approximate $1e^-$ capacity of 150 mAh. The cathode thickness was $\sim$1 mm. Both cells were initially discharged at 0.5 mA/cm^2. The cells exhibited practically no capacity to 1.9V. The currents were then reduced to 0.125 mA/cm^2. Capacities of $\sim$0.05 e^-/V were exhibited by both of the cells to 1.9V cutoff. It appears that both of the oxides cannot be discharged without carbon in the cathode matrix. It is known that $Li_xV_6O_{13}$ becomes an insulator when $x = \sim 4$ (7). In high rate cells, probably an insulating layer of $Li_xV_6O_{13}$ is formed in the early stages of discharge so that further discharge is not possible.

3.3.2 Effect of Voltage Limits on Cell Cycle Life

All the studies in this section were carried out with the non-stoichiometric oxides. Nevertheless, the results of the next section would suggest that the conclusions are valid for the stoichiometric oxide also.

Cycling Limits of 3.0V and 1.4V. The pressed powder cathode in cell No. 39 contained 0.31g V_6O_{13} (50 w/o), 40 w/o carbon and 10 w/o Teflon. The first two cycles of this cell at 8 mA (0.5 mA/cm^2) are shown in Fig. 9. The cycling data are tabulated in Table 6. The first discharge preceeded in 4 distinct voltage regions. To 1.7V cutoff, the capacity

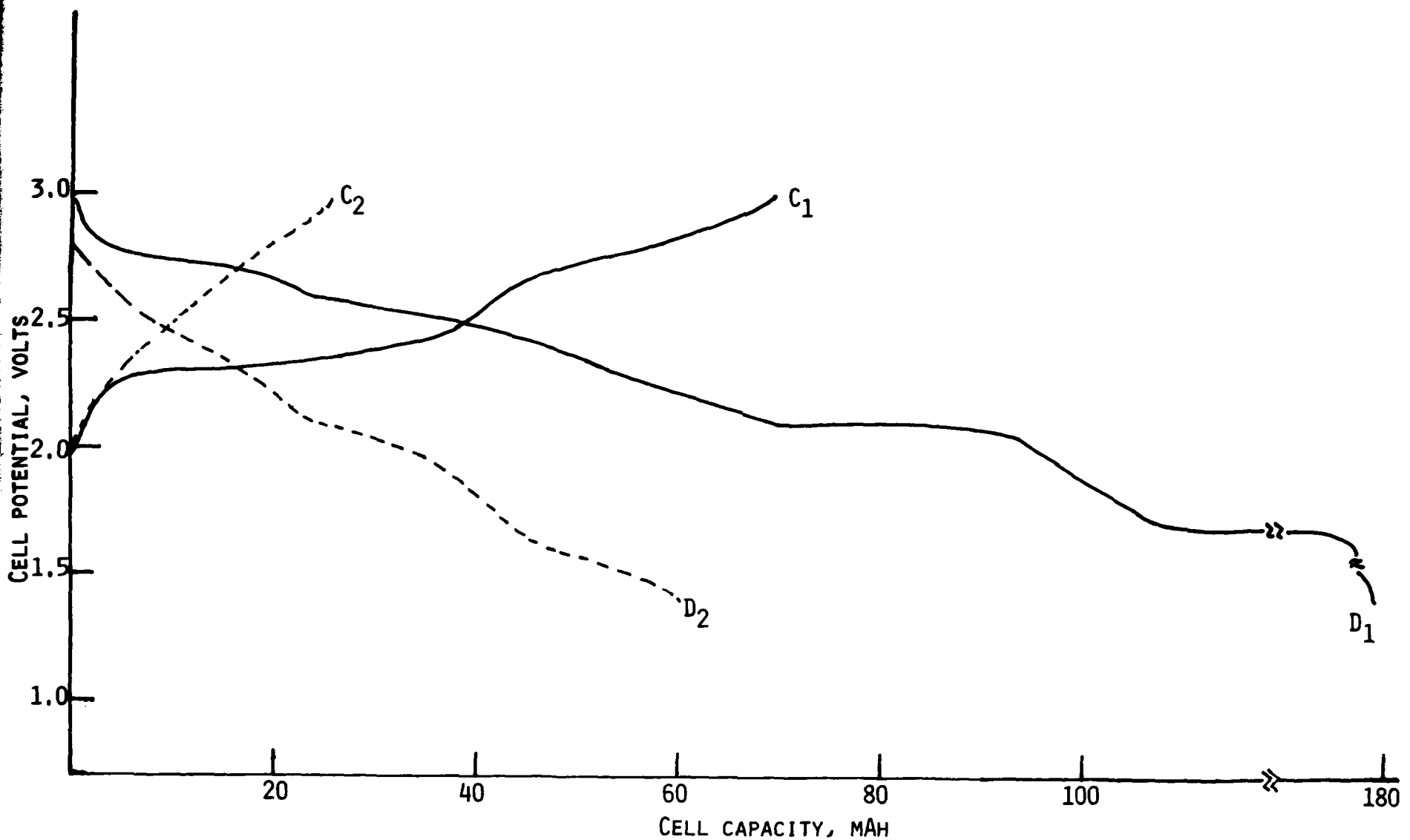

Fig. 9. Galvanostatic cycling curves for Li/V_6O_{13} cell 39. Current = 8 mA (0.5 mA/cm^2). Voltage limits 1.4V and 3.0V

Table 6

Cycling Data for Li/V_6O_{13} Cell No. 39

Cathode: 50 w/o V_6O_{13} (0.31g, 3.8 mmoles), 40 w/o graphite, 10 w/o Teflon.

Current: 8 mA (0.5 mA/cm^2).

Cycle No.	Discharge Capacity		Charge Capacity	
	mAh	e^-/V	mAh	% of Discharge
1	191	1.87	70	37
2	65	0.64	26	40
3	22	0.22	12	55
4	12	0.12	8	67

corresponded to 112 mAh (1.1 e^-/V). However, an additional capacity of 66 mAh (0.65 e^-/V) was obtained at the lower voltage region between 1.7V and 1.4V. Note that the total discharge capacity of 1.75 e^-/V (10.5 e^-/V_6O_{13}) to 1.4V exceeds the capacity determined from chemical lithiation, i.e., 7.8 e^-/V_6O_{13}. This appears to indicate that at the lower voltage region further reduction of the oxide occurs. The first charge corresponded to 70 mAh (4.1 e^-/V_6O_{13}) which was 39% of the charge utilized in the first discharge. The capacity decreased with cycles reaching 12 mAh by the 4th discharge.

Cycling Limits of 3.0V and 1.7V. This was evaluated in cell No. 52. The oxide was non-stoichiometric. The cycling data are tabulated in Table 7. Representative cycles are shown in Figure 10. A plot of cathode utilization vs. cycle no. is depicted in Fig. 11. The cathode utilization in the first discharge was 113% of theoretical capacity based on $6e^-/V_6O_{13}$. In the first charge 76% of this capacity was recharged. Although the cathode utilization gradually decreased with cycle number, the dramatic cathode failure observed with the 1.4V lower limit was eliminated.

Cycling Limits of 3.5V and 1.7V. Two cells were evaluated, cell Nos. 57 and 67. The cycling data are listed in Tables 8 and 9, respectively.

Cell No. 57 was initially cycled between 3.0V and 1.7V. The cathode utilization in the first discharge was 0.95 e^-/V. In the first charge 84% of this capacity was recharged. Further capacity loss with cycling was again gradual (see Fig. 11). At the 10th charge half cycle, the upper voltage limit was raised to 3.5V. The charge capacity slightly increased with subsequent discharges also showing slightly improved cathode utilization. However, the declining trend in cathode utilization with cycle number was not eliminated.

Cell No. 67 was cycled between limits of 3.5V and 1.7V. The performance of the cell was similar (see Table 9 and Fig. 11) to that of cell No. 52 cycled between 3.0V and 1.7V.

Cycling Limits of 3.0V and 1.9V. In cell No. 73, the voltage limits were 3.0V and 1.9V. Cycling data are given in Table 10. The cathode utilization in the first discharge was 0.9 e^-/V, slightly lower than in the other cells. However, this lower utilization may reflect the higher discharge voltage limit. By the 3rd cycle the cathode utilization decreased to 0.65 e^-/V. However, a capacity >0.5 e^-/V was maintained up to the 16th cycle (see Fig. 11) when the cell was terminated.

Cycling data for cell No. 105, shown in Fig. 12, further substantiates the deleterious effect of deep discharge on cycle life. The cell was cycled at 8 mA (0.5 mA/cm^2). The initial voltage limits were 3.0V and 1.9V. The capacity in the first discharge was 72.3 mAh, equivalent to 0.96 e^-/V. Of this capacity, 82% (0.78 e^-/V) was recharged in the first charge. The capacity in the second discharge corresponded to 0.72

Table 7

Cycling Data for Li/V_6O_{13} Cell No. 52

Cathode: 80 w/o V_6O_{13} (0.48 mmoles), 20 w/o Shawinigan carbon, 5 w/o Teflon

Current: 8 mA (0.5 mA/cm^2)

Voltage limits: 1.7V and 3.0V

	Discharge Capacity		Charge Capacity	
Cycle No.	mAh	% Cathode* Utilization	mAh	% of Discharge
1	87	113	66	76
2	60	78	58	97
3	57	74	58	101
4	55	71	55	100
5	54	70	53	98
6	50	65	48	96
7	45	60	44	98
8	42	54	40	95
9	40	51	38	95
10	36	47	35	97
11	36	47	34	95

*Based on $6e^-/V_6O_{13}$.

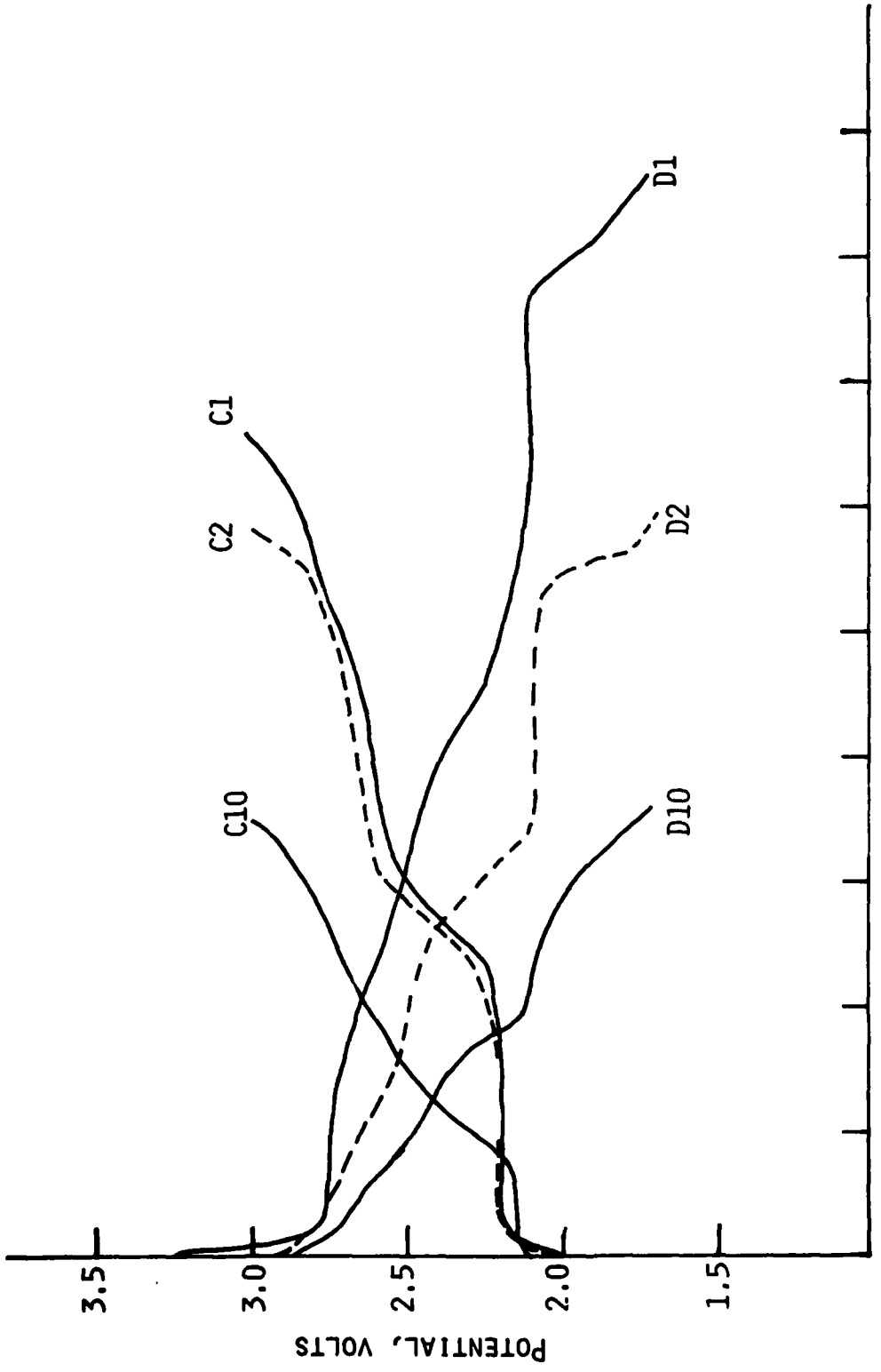

Fig. 10. Galvanostatic cycling curves for Cell No. 52 showing the 1st, 2nd and 10th cycles. Current = 8 mA (0.5 mA/cm^2). Voltage limits, 1.7V and 3.0V.

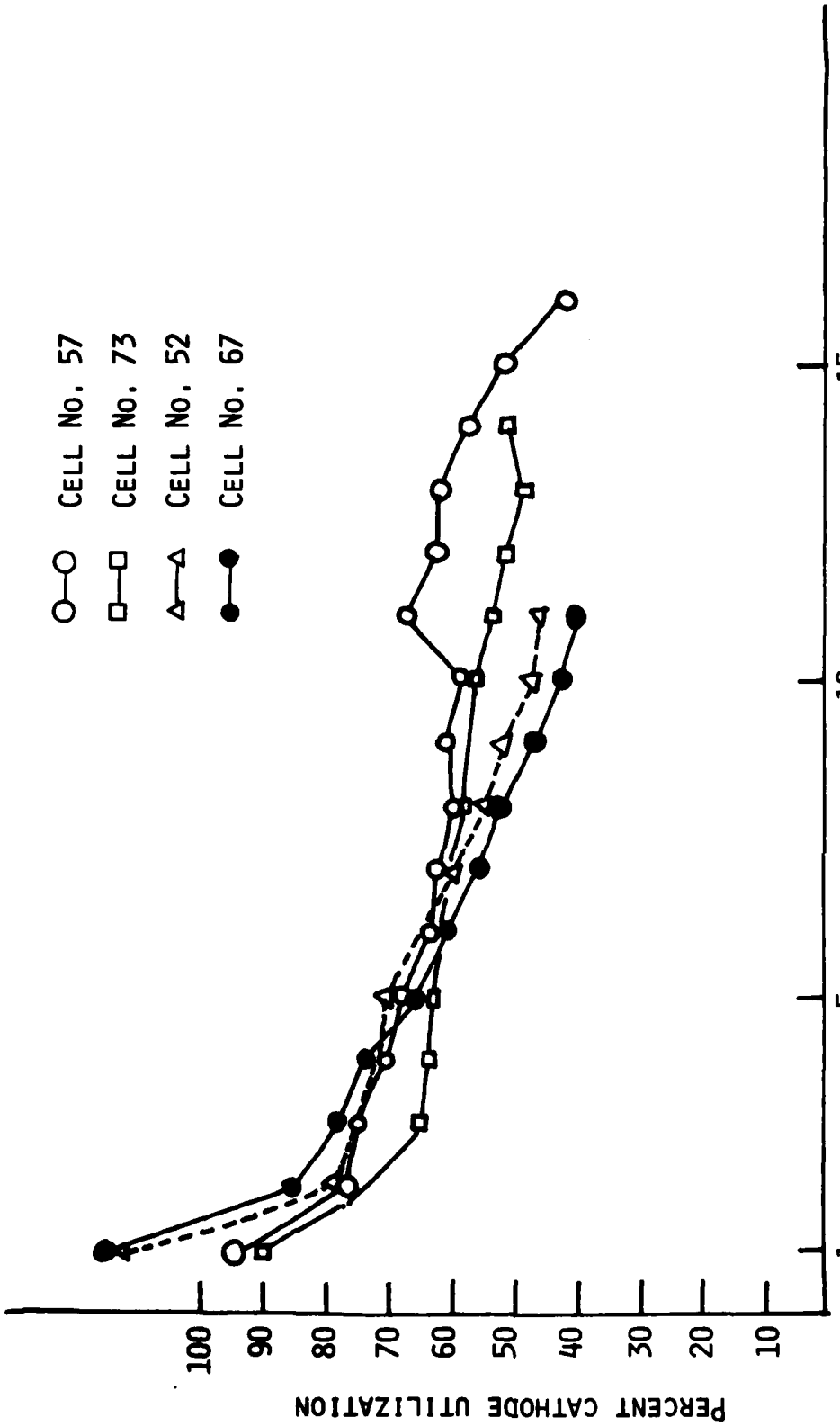

Fig. 11 Percent cathode utilization vs. cycle no. for Li/V_6O_{13} cells. 100% cathode utilization is equivalent to $6e^-/V_6O_{13}$.

Table 8

Cycling Data for Li/V_6O_{13} Cell No. 57

Cathode: 50 w/o V_6O_{13} (0.49 mmoles), 40 w/o AGM graphite, 10 w/o Teflon.

Current: 8 mA (0.5 mA/cm^2).

Voltage limits*: 3.0V and 1.7V.

	Discharge Capacity		Charge Capacity	
Cycle No.	mAh	% Cathode Utilization	mAh	% of Discharge
1	74	95	62	84
2	60	77	58	97
3	58	75	57	98
4	55	70	54	98
5	53	68	51	96
6	49	63	49	100
7	48	62	47	98
8	46	59	46	100
9	47	61	46	98
10	45	58	53*	117
11	53	68	57	107
12	48	62	47	98
13	48	62	45	94
14	44	57	43	98
15	44	57	41	93
16	46	52	38	95

*The upper limit raised to 3.5V from the 10th charge onwards.

Table 9

Cycling Data for Li/V_6O_{13} Cell No. 67

Cathode: 50 w/o V_6O_{13} (0.49 mmoles), 40 w/o AGM graphite, 10 w/o Teflon.

Current: 8 mA (0.5 mA/cm^2).

Voltage limits: 3.6V and 1.7V.

	Discharge Capacity		Charge Capacity	
Cycle No.	mAh	% Cathode Utilization	mAh	% of Discharge
1	90	115	71	79
2	66	87	64	97
3	61	78	59	97
4	57	73	54	95
5	52	67	49	94
6	47	61	45	96
7	42	54	40	95
8	41	52	38	93
9	37	47	34	92
10	33	42	29	88
11	31	40	30	97

Table 10

Cycling Data for Li/V_6O_{13} Cell No. 73

Cathode: 50 w/o V_6O_{13} (0.49 mmoles), 40 w/o AGM graphite, 10% Teflon.

Current: 8 mA (0.5 mA/cm^2).

Voltage limits: 1.9V and 3.0V.

	Discharge Capacity		Charge Capacity	
Cycle No.	mAh	% Cathode Utilization	mAh	% of Discharge
1	71	90	-	-
2	-	-	52	-
3	51	65	52	102
4	50	64	50	100
5	49	63	48	98
6	48	62	47	98
7	48	62	47	98
8	46	59	45	98
9	-	-	-	-
10	42	57	44	105
11	40	53	41	102
12	48	51	40	100
13	38	49	39	103
14	40	51	37	93
15	37	47	36	97

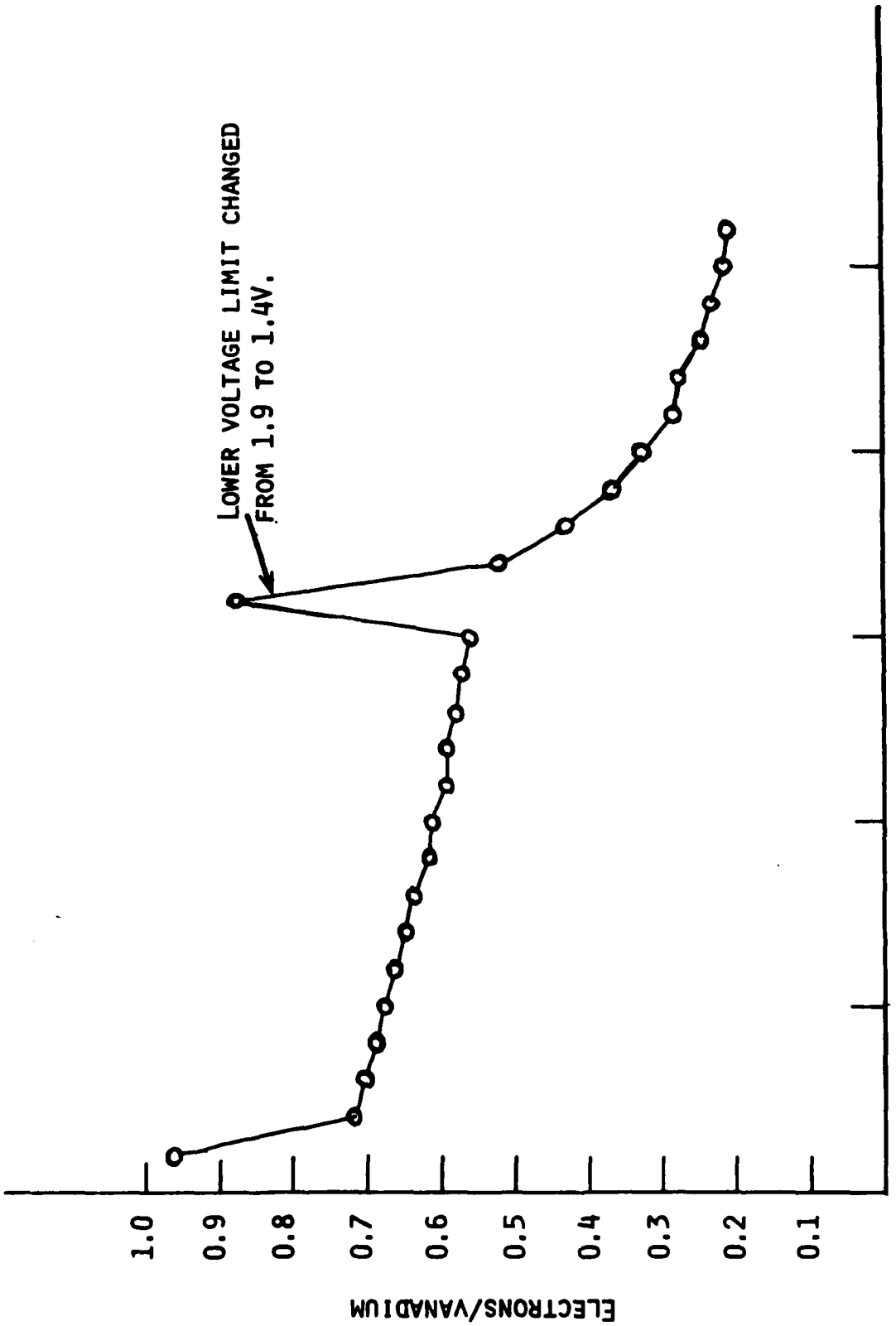

Fig. 12. Cathode utilization vs. cycle number for Li/V_6O_{13} Cell No. 105. Current = 8 mA (0.5 mA/cm^2). For cycles 1-15 voltage limits were 3.0V and 1.9V. For cycles 16-26 voltage limits were 3.0V and 1.4V.

e^-/V which gradually decreased to 0.56 e^-/V by the 15th cycle. About 1% of the capacity is lost in each discharge. At the 16th discharge, the lower voltage limit was set at 1.4V. An additional capacity of 0.32 e^-/V was obtained. However, in subsequent cycles the capacity decreased drastically, loosing about 3.6% per discharge. It thus appears reversible damage to the cathode is induced by deep discharge to 1.4V.

The above results suggest that the rechargeability of V_6O_{13} cathode is very sensitive to lower cell voltage limit. The safe limit appears to be 1.7V. Raising the upper voltage limit from 3.0V to 3.5V did not seem to improve cell cycle life. Although an upper limit of 3.5V did not have a significant deleterious effect on cell cycle life, a safe upper cutoff voltage which will permit good rechargeability for the cathode and at the same time avoid electrolyte degradation appears to be between 3.0V and 3.2V. It should be pointed out that studies of Koch, et al., (11) indicated that significant anodic decomposition of 2Me-THF/$LiAsF_6$ would occur only at potentials $\geq$4.2V.

One of the reasons for the decreasing cathode utilization even within the cycling limits of 3.0 and 1.9 volts may be the formation of localized resistive areas in the cell with continued cycling. Note that the non-stoichiometric oxide incorporated 6 Li/V_6O_{13} electrochemically, but the semiconductor to the insulator phase transition occurs at a Li capacity of 4 per V_6O_{13}. In the stoichiometric oxide, as seen later, excellent rechargeability is observed within the cycling limits of 3.0V and 1.9V. In the latter oxide, however, the discharge at ambient temperature does not occur to any significant extent into the insulator phase of the $Li_xV_6O_{13}$ ternary.

3.3.3 Potentiostatic Studies of the Effect of Deep Discharge on Cathode Performance

Potentiostatic discharges of cathodes utilizing the non-stoichiometric and the stoichiometric oxides were performed to evaluate the nature of electrode processes at potentials between 1.3V and 1.9V. Each cathode was initially discharged at 1.9V and then the potential was lowered to 1.3V at 0.1V interval. At each potential the current was allowed to decay to <10 μA. A plot of the net capacity at each potential is shown in Fig. 13. A capacity versus current density plot for each of the oxides at the 1.9V and 1.6V discharges are shown in Fig. 14 and 15 respectively. The capacity at the 1.9V discharge corresponded to 1.17 e^-/V for the non-stoichiometric oxide and 0.71 e^-/V for the stoichiometric oxide. At 1.8V and 1.7V very little additional capacities were obtained. At 1.6V, however, substantially additional capacities were observed in both cathodes indicating further reduction processes. The additional capacity for the stoichiometric oxide at 1.6V was 1.46 e^-/V whereas that for the non-stoichiometric oxide was 0.71 e^-/V. This substantial difference tends to suggest that the discharge process at 1.6V is due to the cathode material and not the solvent. This is further substantiated by the observation that

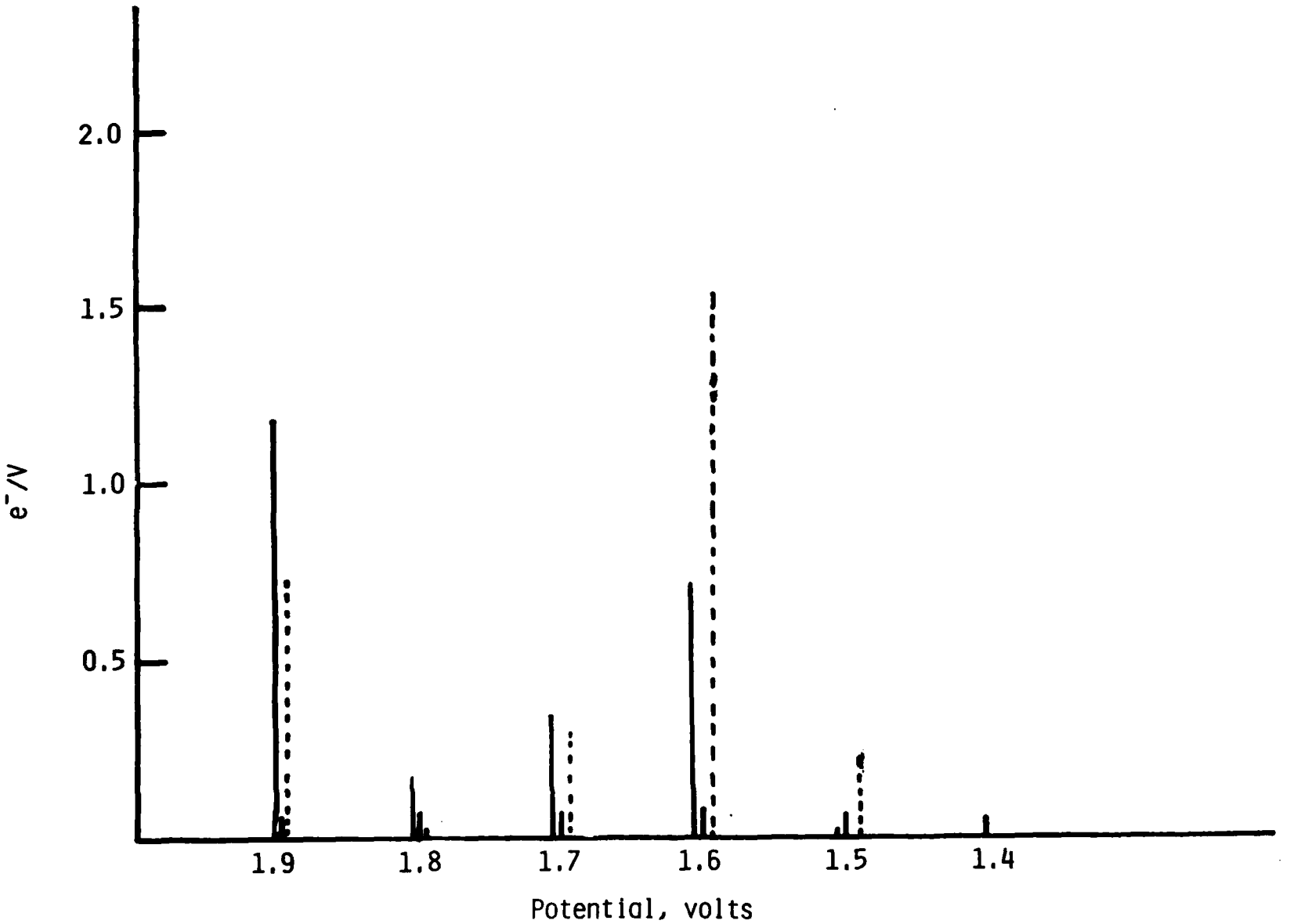

Fig. 13. Capacities at various potentials of V_6O_{13} cathodes potentiostated decrementally at potentials beginning with 1.9V.

—— non stoichiometric oxide.

---- stoichiometric oxide.

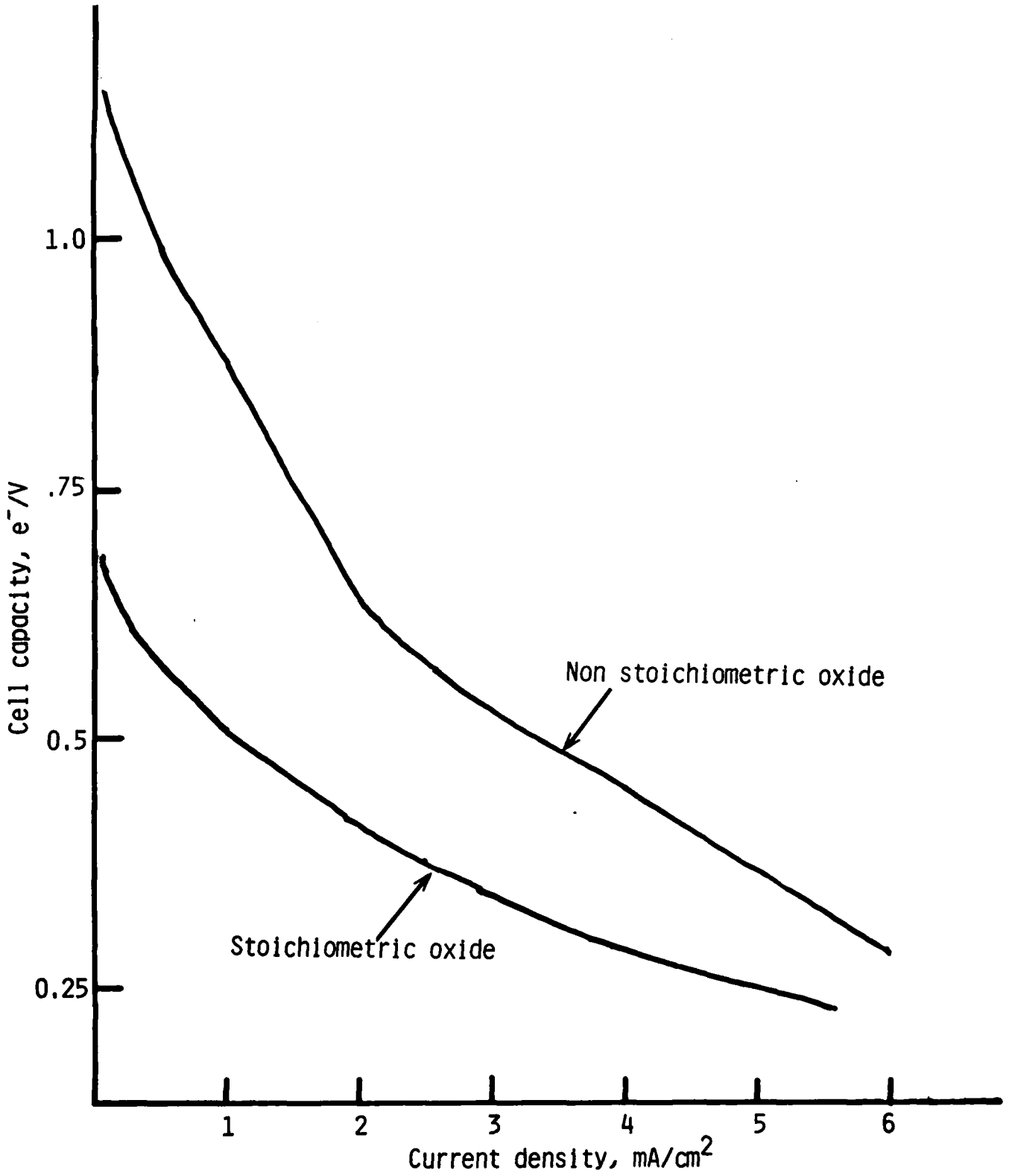

Fig. 14. Capacity vs. current density for the stoichiometric and non-stoichiometric oxides potentiostated at 1.9V.

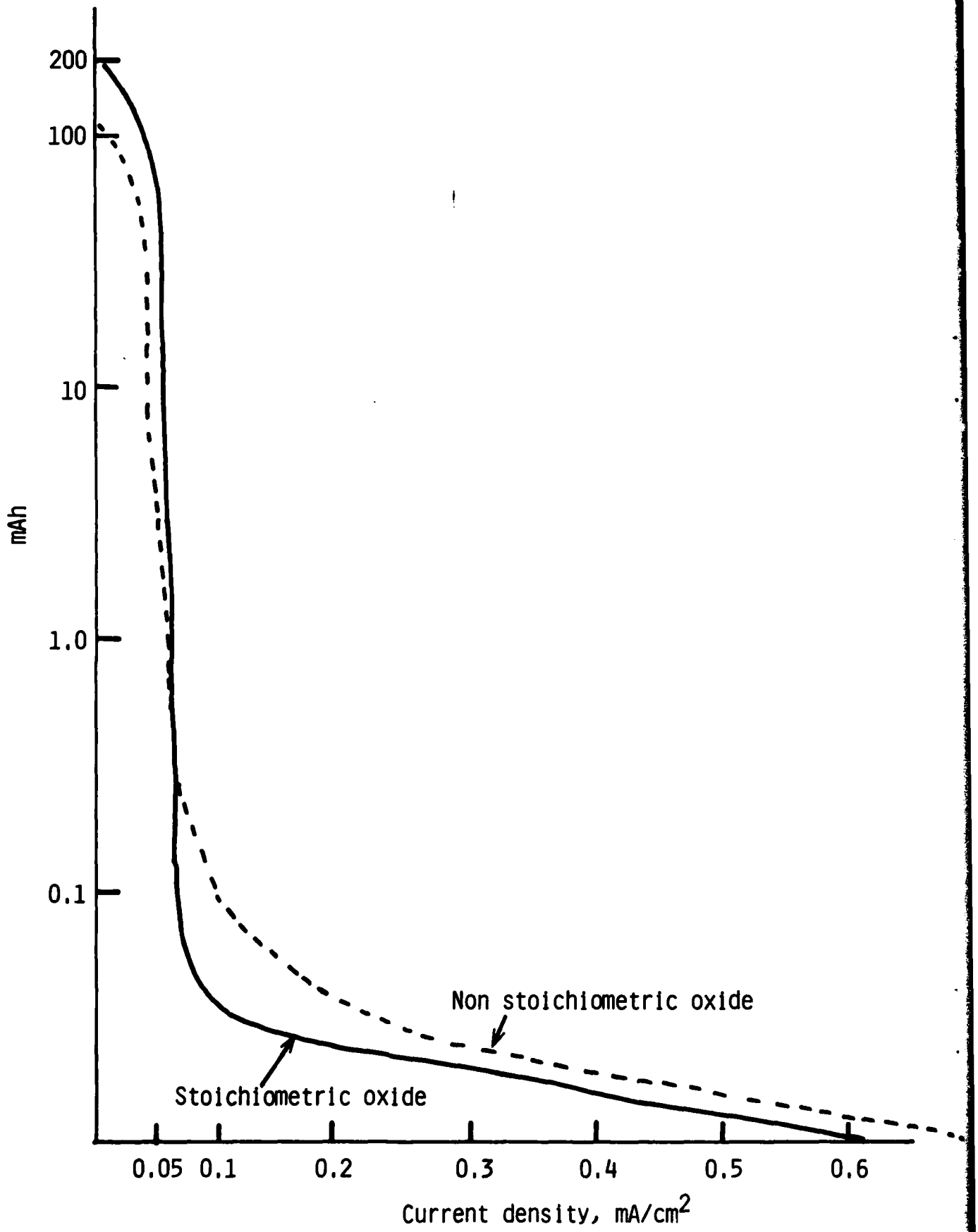

Fig. 15. Capacity versus current density for vanadium oxide cathodes potentiostated at 1.6V after the discharges at 1.9, 1.8 and 1.7 volts.

the electrolyte itself does not show substantial current on a carbon electrode up to 1.3V (13). The integrated capacities of the two oxides from the potentiostatic discharges at 1.9, 1.8, 1.7 and 1.6V were remarkably close, being 360 mAh for the non-stoichiometric oxide and 374 mAh for the stoichiometric oxide. This capacity corresponds to 14 e^-/V_6O_{13}, being equivalent to the reduction of all the vanadium ions to V^{+2}.

Very low capacities were obtained at 1.5, 1.4 and 1.3 volts. The cathodes could not be charged potentiostatically after the high capacity reduction at 1.6V. The data suggest that the cathode undergoes an irreversible reduction at ∿1.6V which appears to be the reduction of vanadium ions to V^{+2}.

3.3.4 Cycling of $Li_{7.8}V_6O_{13}$

Cycling behavior of $Li_{\sim 8}V_6O_{13}$, prepared from nBuLi and V_6O_{13} was evaluated to assess the effect of lower voltage Li intercalation into V_6O_{13}. (The potential of nBuLi vs. Li is about 1.0V.) The open circuit potential of the cell was 2.05V. The cell resistance was 2.15Ω as in cells with V_6O_{13} cathode. The cell was initially charged to 3.0V at 0.5 mA/cm^2 and then cycled at the same rate between voltage limits of 1.9V and 3.0V. The first charge corresponded to only 0.47 e^-/V. The cathode virtually showed irreversible behavior as shown by the data in Table 11. It is apparent that incorporation of more than ∿6 Li into the V_6O_{13} structure significantly affect the rechargeability of the cathode.

3.4 Cathode Optimization Studies

A limited amount of cathode optimization studies were carried out. Specifically, we investigated the following: a) effect of cathode composition, i.e., V_6O_{13} to C ration, on utilization; b) effect of cathode pressing parameter on utilization; c) effect of cathode thickness on rate-capacity behavior.

3.4.1 Vanadium Oxide to Carbon Ratio

The need for carbon in the electrode matrix has already been shown. However, an unacceptably large amount of carbon will substantially reduce the volumetric energy density. Although a detailed matrix analysis of the effects of carbon on utilization and cycle life has not been carried out. A cathode mix consisting of ∿20 w/o of the 50% compressed Shawinigan carbon appears to be the optimum. This is borne out by the rate-capacity studies discussed below in Section 3.4.3.

3.4.2 Effect of Cathode Pressing Parameter on Utilization

In cells #280-033 and #280-085 the cathodes were fabricated with 70 w/o non-stoichiometric V_6O_{13}, 20 w/o C and 10 w/o Teflon. However,

Table 11

Cycling Data for Li/V_6O_{13} Cell No. 131

Cathode: 50 w/o $Li_8V_6O_{13}$ (0.20g, 0.35 mmole), 40 w/o graphite, 10 w/o Teflon.

Current: 8 mA (0.5 mA/cm^2).

	Discharge Capacity		Charge Capacity
Cycle No.	mAh	Cathode Utilization, e^-/V	mAh
1	-	-	26.7 ($0.47e^-/V$)
2	13.6	0.24	12.8
3	11.5	0.20	11
4	10.9	0.19	9.7
5	9.5	0.17	9.1
6	8.3	0.15	8.3
7	8.3	0.15	7.9
8	8.3	0.15	7.3
9	7.3	0.13	7.9
10	7.3	0.13	7.0

- The cell was charged first.

the cathode in cell #280-033 was pressed at 1000 lbs/in^2 and the cathode in cell #280-085 was pressed at 5000 lbs/in^2. The cycling data are shown in Fig. 16 plotted as cathode utilization versus cycle number. There is practically no difference in the performances of the two cells. In most of the cells evaluated in this study, the cathodes were therefore pressed at $\sim$2000 lbs/in^2.

3.4.3 Rate-Capacity Studies

Rate-capacity studies were carried out with both types of the oxide, although the more detailed investigation utilized the stoichiometric oxide. This was because of the high reversibility of this oxide even in the first cycle so that one cell could be used for a series of rate-capacity measurements.

Stoichiometric V_6O_{13}. Capacities were obtained at current densities of 8, 6, 4, 2, 1 and 0.5 mA/cm^2. The test was started with the highest rate. After each discharge the cell was charged to 3.0V at 0.5 mA/cm^2 to obtain the capacity at the next rate. The capacities at the various current densities were obtained as a function of cathode thickness using cathodes of 28, 51 and 73 mil thick. They had theoretical capacity (1 e^-/V) densities of 10, 20.8 and 30.5 mAh per cm^2 respectively.

Discharge curves for the cell utilizing the 20.8 mAh/cm^2 cathode are shown in Fig. 17. Plots of cathode utilization as a function of electrode thickness at each current density are shown in Fig. 18. Plots of cathode utilization versus current density for the three cathodes are depicted in Fig. 19.

For the 51 mil thick cathode, a capacity of 0.58 e^-/V was obtained at current densities of 0.5, 1.0 and 2.0 mA/cm^2. At 4 mA/cm^2, the capacity was 0.48 e^-/V. The practically similar capacities at current densities $\leq$2.0 mA/cm^2 suggest that the electrolyte transport properties have very little effect on cathode utilization at these currents. The electrolyte transport properties appear to affect cathode utilization at higher currents. For example, the 4.0 mA/cm^2 discharge for the 51 mil thick cathode and the 2.0 mA/cm^2 discharge for the 29 mil thick cathode correspond to the same rate. But the capacities show a significant difference.

For the 51 mil thick cathode with a Li cycling efficiency of 97%, the calculated volumetric energy density is $\sim$260 Whr/Dm^3 at current densities $\leq$4.0 mA/cm^2. This does not take into account the volume required for the electrolyte.

Non-stoichiometric V_6O_{13}. Figure 20 shows the capacities in the first discharge as a function of current density. All the cathodes were of $\sim$25 mil thickness. A large number of cells have been discharged at 0.5 mA/cm^2. In these cells, the capacities in the first discharge varied from 0.94 e^-/V to 1.1 e^-/V. Only one cell each was discharged at the other current densities. Virtually identical capacities are

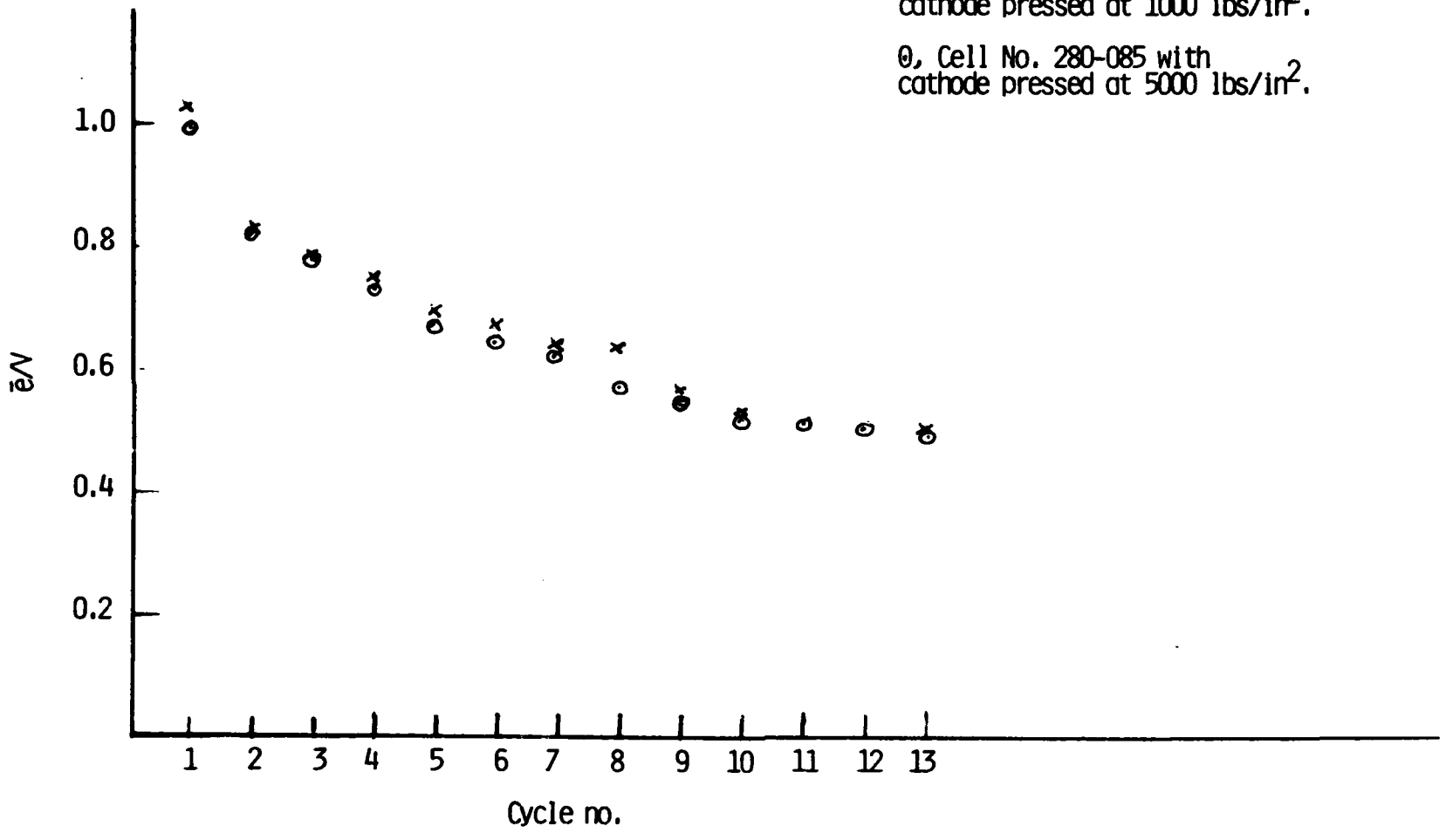

Fig. 16. Cathode utilization versus cycle no. for two Li/V_6O_{13} cells utilizing non-stoichiometric oxide.

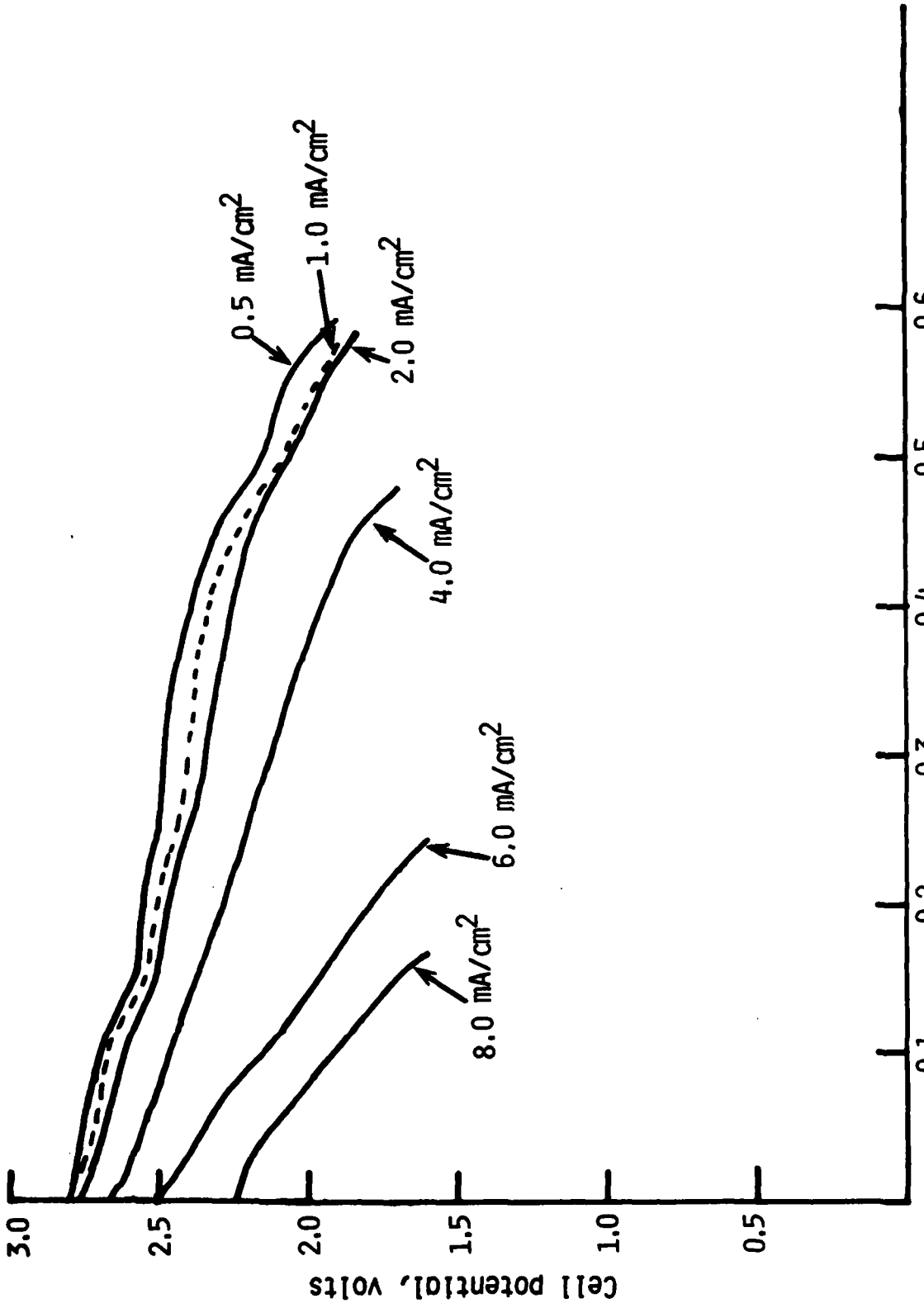

Fig. 17. Capacities of the Li/V_6O_{13} cell utilizing stoichiometric V_6O_{13} at various current densities. Cathode has 313 mAh (1e⁻) capacity. Cathode thickness = 51 mils. Cathode area = 15.5 cm^2 for both sides.

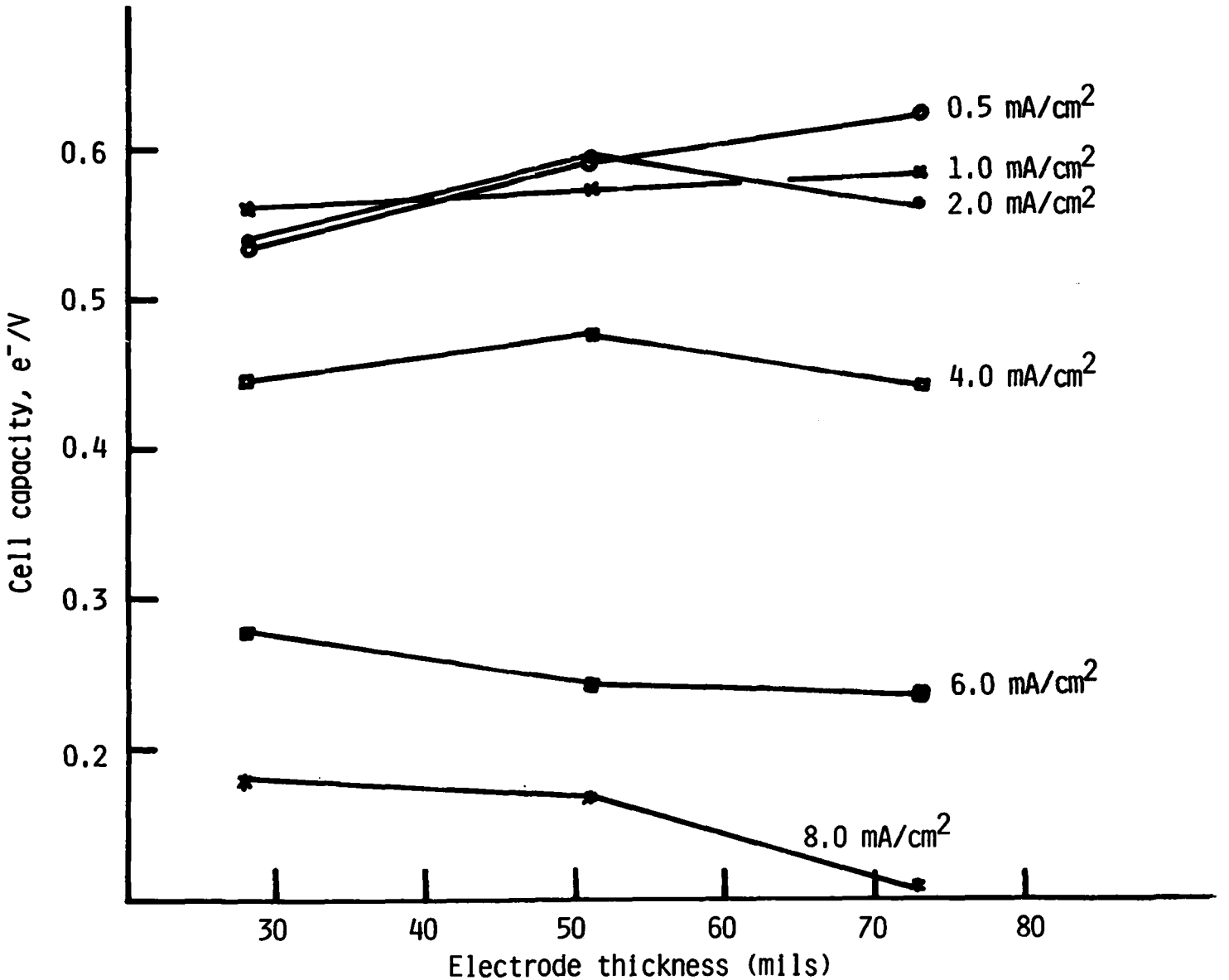

Fig. 18. Cathode utilization, e^-/V, at various current densities as a function of thickness. Cathode area = 15.5 cm^2 for both sides. The $1e^-$ capacity and thickness of the electrode are: 52 mAh (28 mils); 313 mAh (51 mils) and 458 mAh (73 mils).

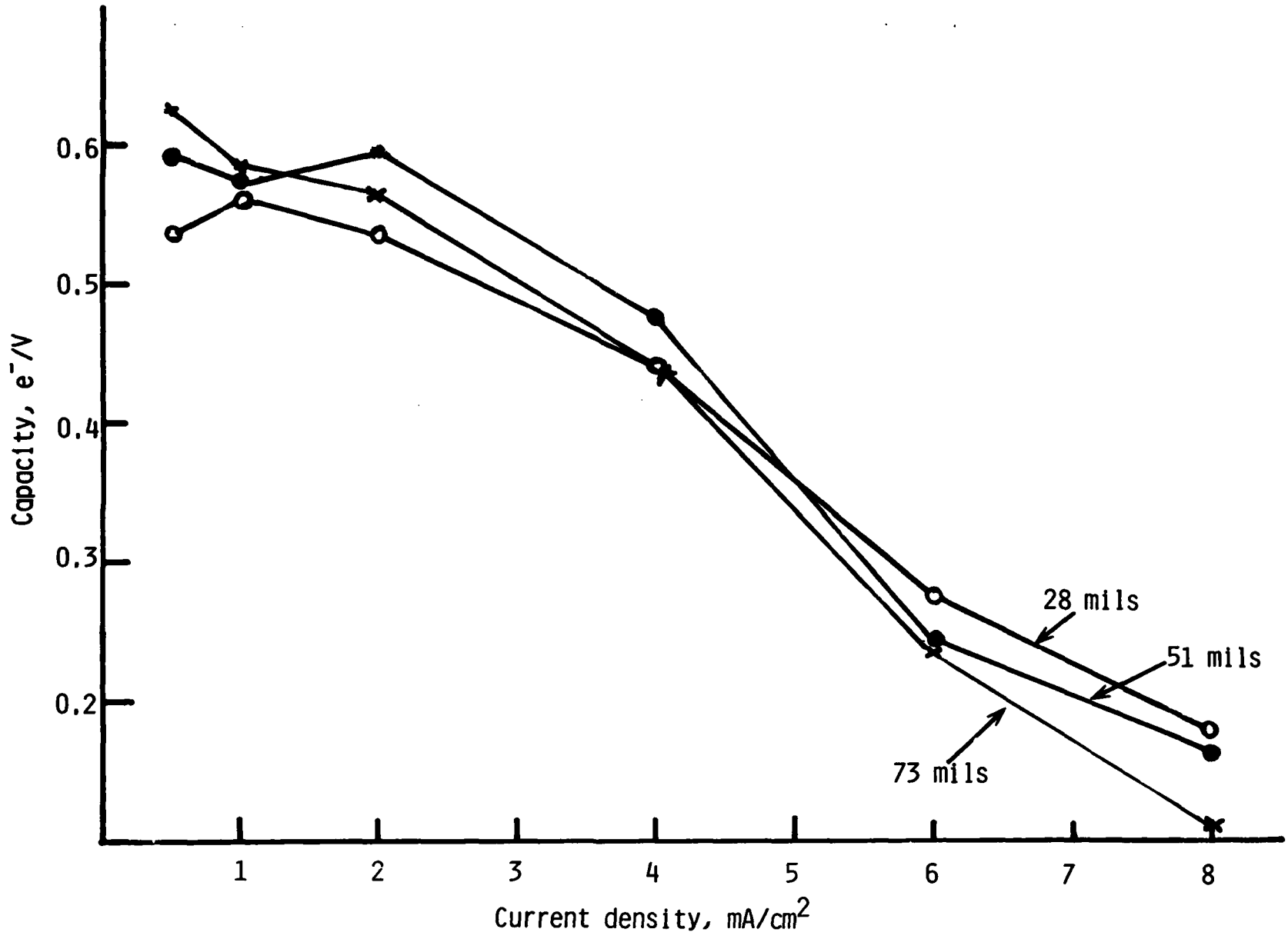

Fig. 19. The cathode utilization at various current densities for the three electrodes shown in Fig. 18.

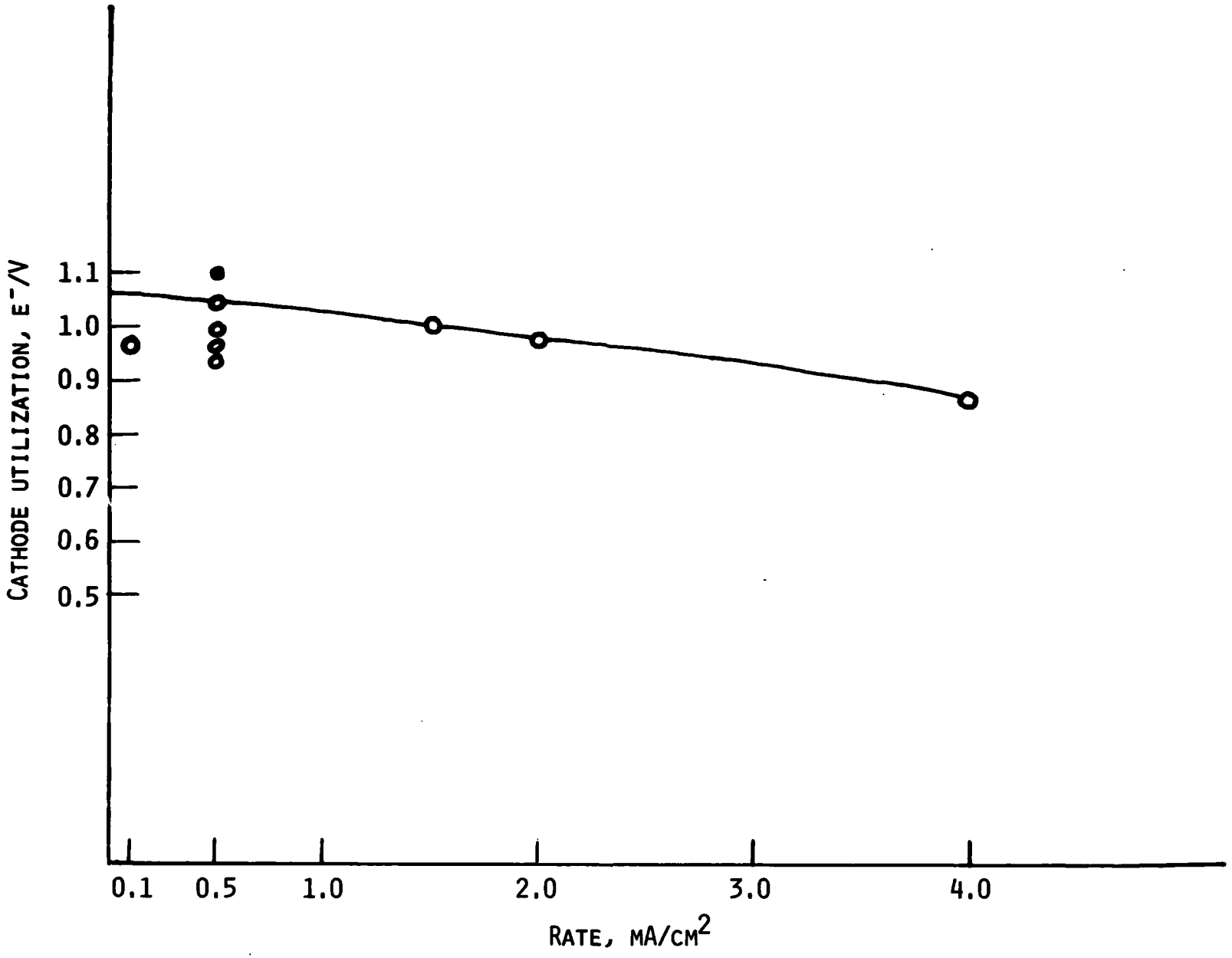

Fig. 20. Capacity-rate behavior of Li/V_6O_{13} cells.

obtained up to a current density of 2 mA/cm^2. This behavior is identical to that of the stoichiometric oxide. At 4 mA/cm^2, the cathode utilization was 0.87 e$^-$/V, i.e., ∿85% of the capacity at ≤2 mA/cm^2, again similar to that of the stoichiometric oxide.

These results suggest Li cells with V_6O_{13} cathodes potentially have high rate capabilities. An amount of ∿20 w/o carbon in the cathode matrix appears to be sufficient for obtaining these high rate performances. At current densities ≤2.0 mA/cm^2, the thickness of the cathode, in the range investigated, has very little effect in utilization.

3.5 Extended Cycling of Li/V_6O_{13} Cells

Rechargeability of the vanadium oxide cathodes were evaluated by extended cycling. These studies were carried out in laboratory glass cells. The cells were cycled galvanostatically between voltage limits of 3.0 and 1.9.

3.5.1 Non-Stoichiometric V_6O_{13}

The cathode in cell No. 255-45, incorporating 70 w/o V_6O_{13}, 20 w/o carbon and 10 w/o Teflon, had a theoretical capacity (1 e$^-$/V) of 83 mAh (5·53 mAh/cm^2 per side). The cell was cycled between voltage limits of 3.0V and 1.9V at current densities of 1.5 mA/cm^2 (23 mA total current) for discharge and 1.0 mA/cm^2 (15.5 mA total current) for charge. A plot of cathode utilization vs. cycle number is shown in Fig. 21. Some typical cycles are shown in Fig. 22. The capacity in the first discharge was 1.1 e$^-$/V. In the second discharge, the capacity decreased to 0.88 e$^-$/V. This loss is due to the inefficiency in the first charge, equalling 20% of the first discharge. With further cycling the capacity showed a continued but slow decline, diminishing to 0.66 e$^-$/V at the 19th discharge. The charge current density was reduced to 1.0 mA/cm^2 at the 19th charge. The cathode rechargeability did not improve. The cathode utilization remained fairly steady at ∿0.63 e$^-$/V up to the 39th discharge. At the end of the 39th discharge a malfunction of the cycler caused the cell to deep discharge to <1.0V causing a drastic reduction in capacity in subsequent cycles. The average cathode utilization in the first 39 cycles was ∿0.7 e$^-$/V.

An identical cell, No. 255-47, was cycled between 3.0V and 1.8V at a current density of 2.0 mA/cm^2 for both discharge and charge. The cathode utilization in the first discharge was 0.98 e$^-$/V which decreased to 0.67 e$^-$/V in the second discharge. The discharge capacity continued to decrease with cycling, diminishing to 0.25 e$^-$/V by the 25th cycle. Between the 25th and the 90th cycles, the capacity essentially remained constant at an average value of 0.21 e$^-$/V. The current density was then reduced to 0.5 mA/cm^2 for both discharge and charge. As a result the cathode utilization increased to 0.49 e$^-$/V. In the next 8 cycles the cathode utilization remained steady at an average value of ∿0.46 e$^-$/V.

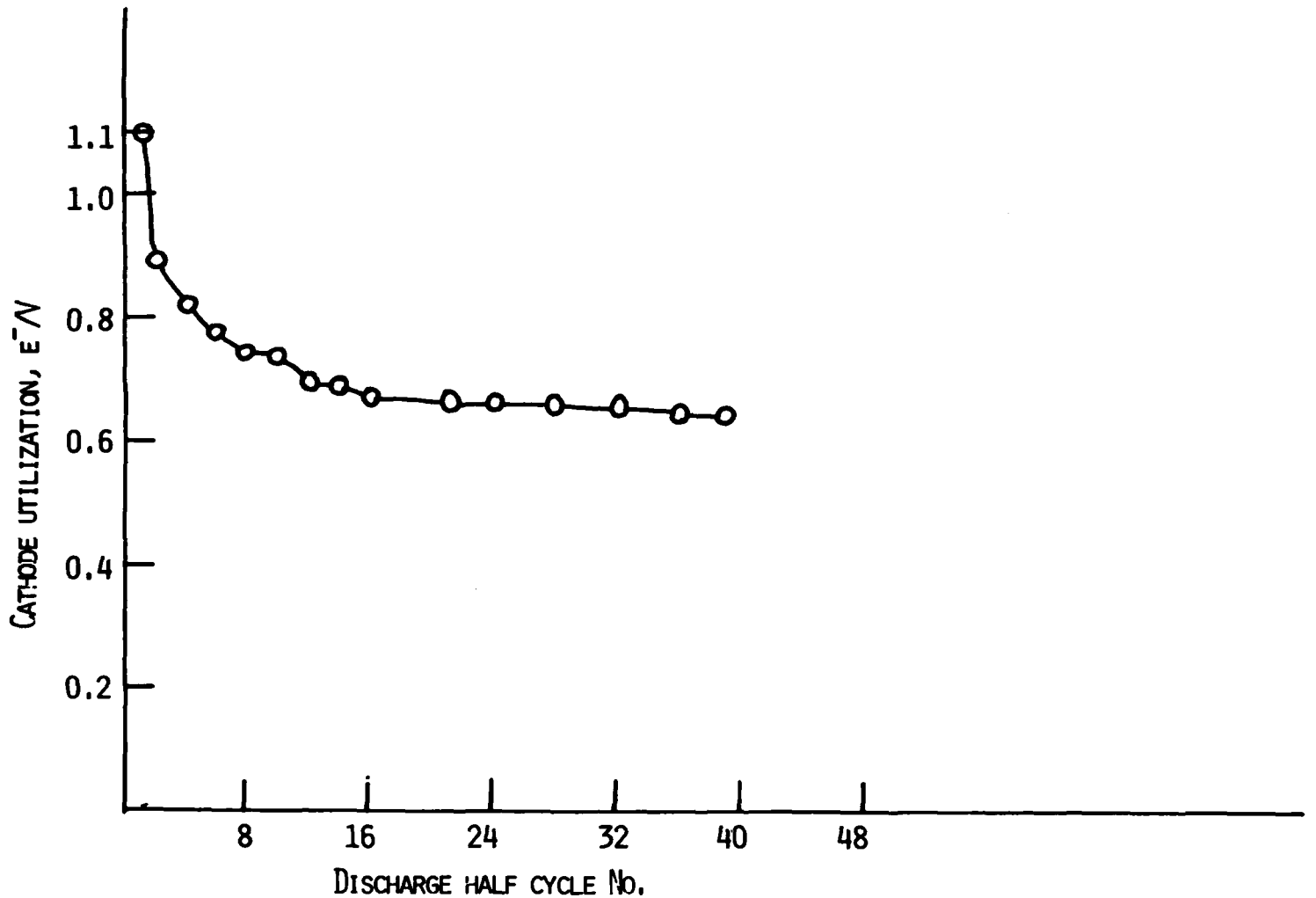

Fig. 21 Cathode utilization vs. cycle number for Li/V_6O_{13}, Cell No. 255-45.

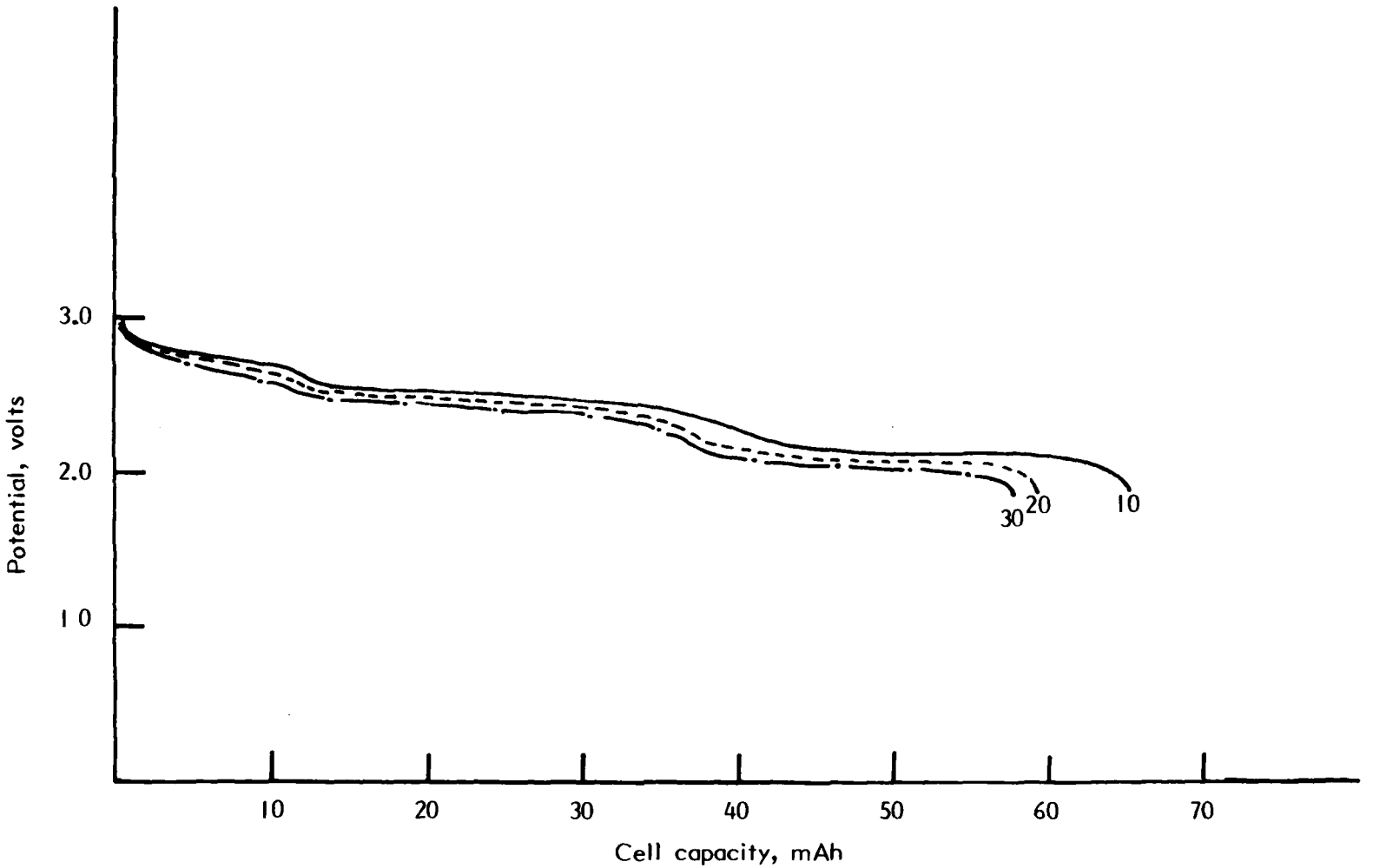

Fig. 22. Typical cycles of Li/V_6O_{13} Cell No. 255-45, utilizing nonstoichiometric oxide.

These extensive cycling studies have demonstrated that the non-stoichiometric oxide has acceptable rechargeability. The following points are noteworthy. A capacity equivalent to ∿15% of the first discharge is not recharged in the first charge. A gradual decline in capacity at a rate of ∿1% per cycle occurs in early cycles subsequent to the second discharge. At lower current densities, i.e., $\leq$1.5 mA/cm^2, this decline seems to be independent of the current density. After the initial decline, however, the capacity seems to stabilize at ∿0.6 e$^-$/V. An effect of rate in cathode utilization was manifested in the cycling at 2 mA/cm^2. A probable reason for the decline in capacity in the early cycles may be related to the insulating characteristics of lithiated phases, $Li_xV_6O_{13}$, $x > 4$. In each cycle a small fraction of the highly lithiated oxide phases probably gets isolated in the electrode matrix and looses electronic contact with the bulk of the material. The electronically isolated material is not electrochemically utilized. Supporting this view is the fact that after the second cycle the potential plateaus of the cycles remain the same despite the lower capacities. It should be possible to remedy this situation by improved cathode fabrication procedures.

3.5.2 Stoichiometric V_6O_{13}

The oxide prepared by the 24 hr heating time was used since this material exhibited the best electrochemical performance. In cell 280-15, a cathode having a theoretical capacity of 147 mAh (based on 1 e$^-$/V) was fabricated from 70 w/o V_6O_{13}, 20 w/o carbon and 10 w/o Teflon. The cell was cycled initially at currents of 22 mA (1·5 mA/cm^2) for discharge and 15 mA (1.0 mA/cm^2) for charge. The voltage limits were 1.9V for discharge and 3.0V for charge. Typical discharges are shown in Fig. 23. Fig. 24 shows a typical cycle. A plot of cathode utilization versus cycle number is shown in Fig. 25.

The first discharge corresponded to 0.47 e$^-$/V. This is slightly lower than the maximum 0.60 e$^-$/V obtainable at room temperature for this oxide. Frequently in pressed powder cathodes which discharge via topochemical reactions, the maximum capacity is not obtained in the first discharge even at low current densities. Indeed, in the second discharge of the present cell, the cathode utilization increased to 0.56 e$^-$/V. With this oxide, however, the first charge is nearly 100% efficient. In cells utilizing the non-stoichiometric oxide, usually ∿15% capacity loss occurs in the first charge.

Cycling rates appeared to have a slight effect on cathode utilization. For example, at the 9th discharge, the current was reduced to 15 mA. The cathode utilization increased from 0.49 e$^-$/V to 0.51 e$^-$/V. Also, reducing the charge current at the 27th cycle to 8 mA (0.5 mA/cm^2), increased the cathode utilization from 0.44 e$^-$/V to 0.48 e$^-$/V. The cell was cycled 80 times and was terminated after the 80th cycle due to a crack in the glass container. The average cathode utilization was 0.45 e$^-$/V.

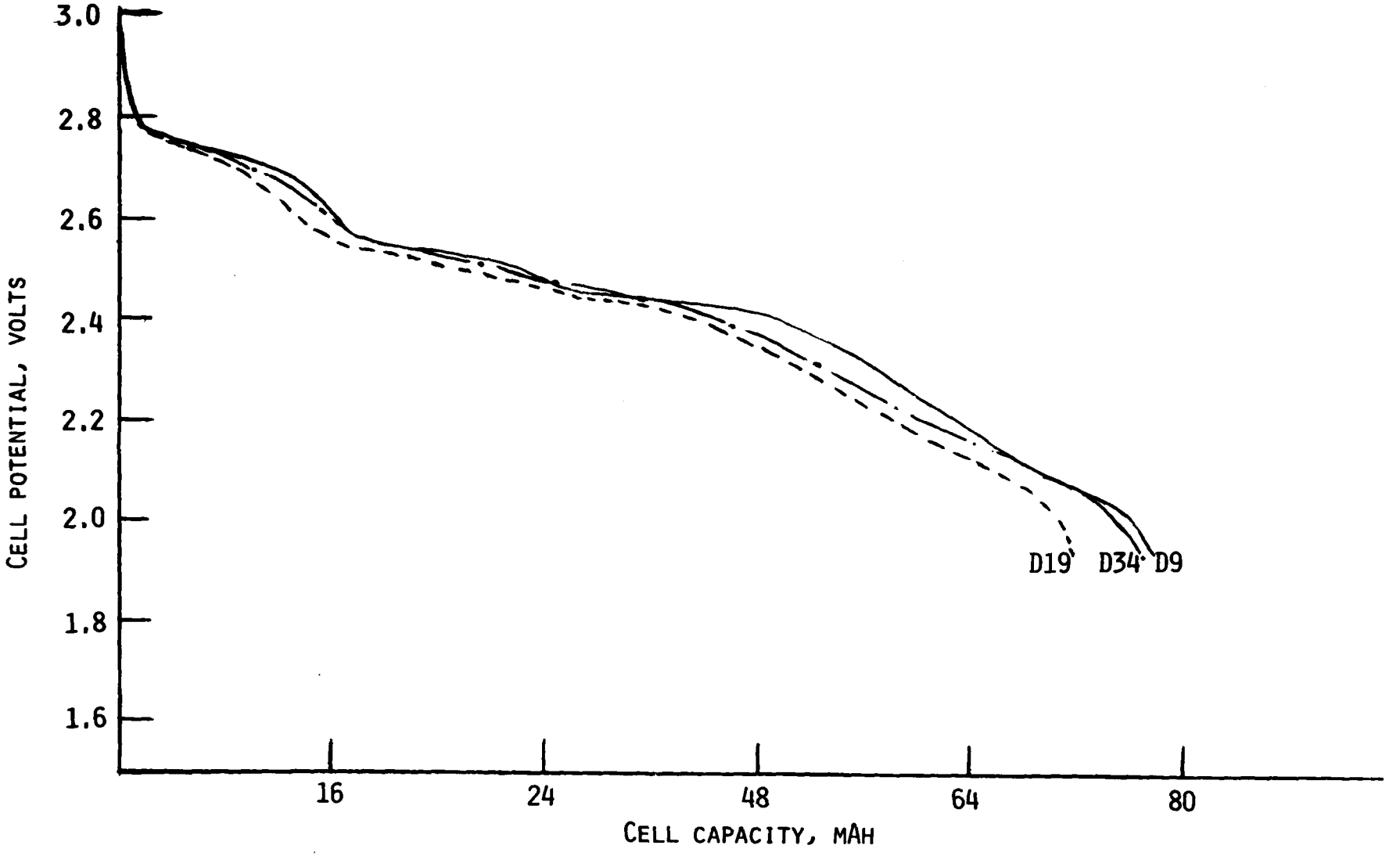

Fig. 23. Typical discharges of Li/V_6O_{13} cell, 280-015 utilizing stoichiometric V_6O_{13}. Current = 15.5 mA (1.0 mA/cm^2).

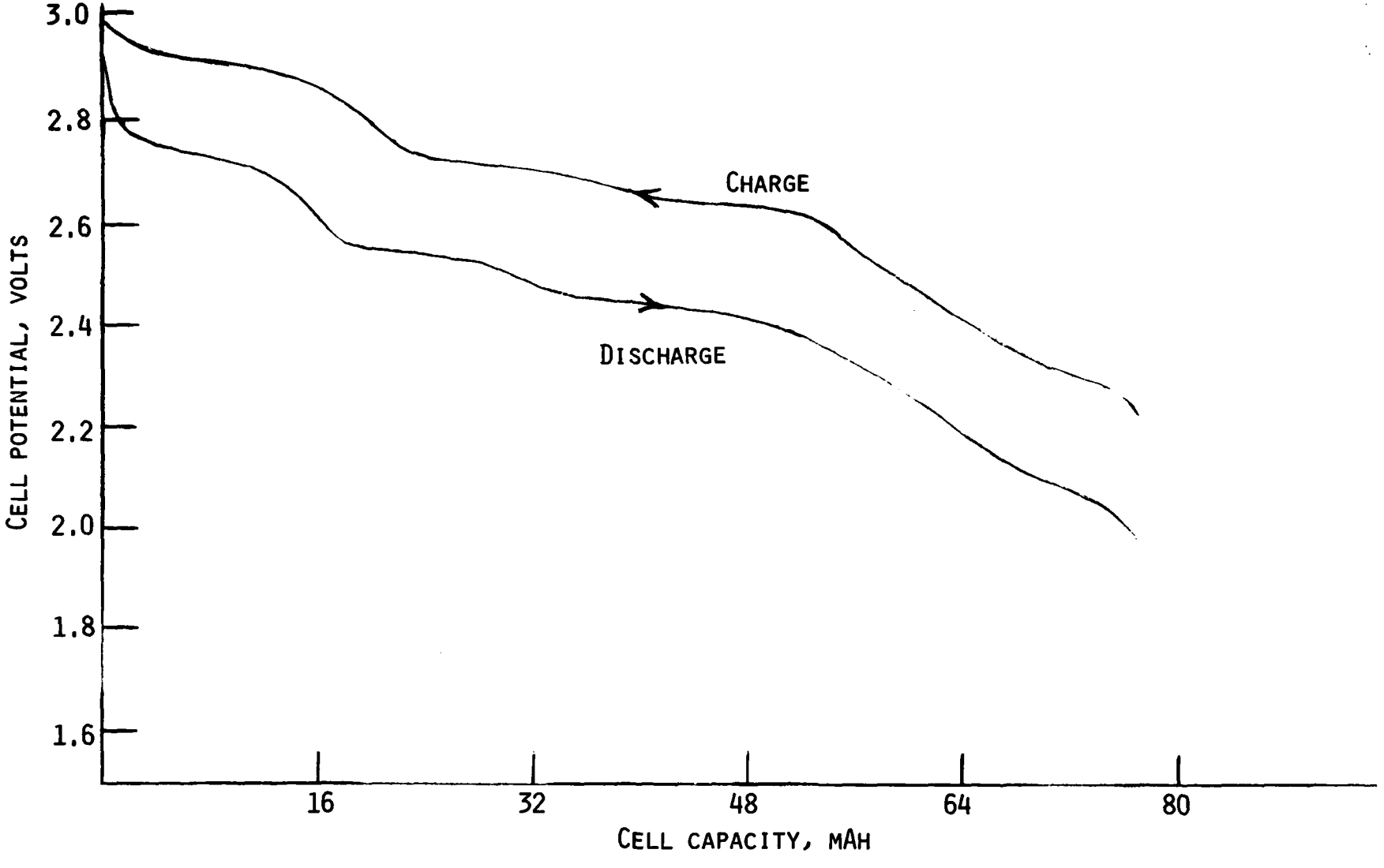

Fig. 24. The 9th cycle of Li/V_6O_{13} cell, 280-015.

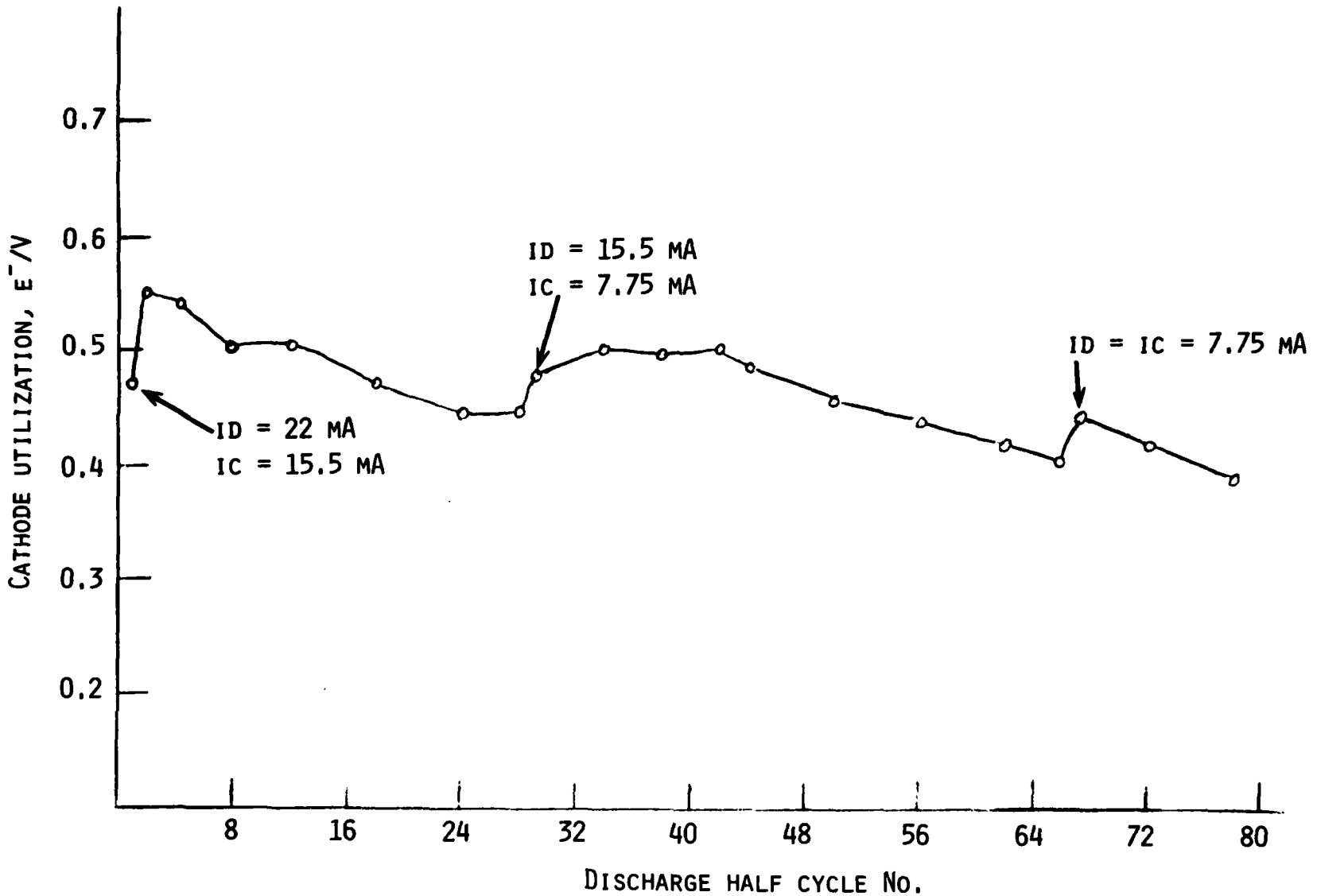

Fig. 25. Cathode utilization as function of cycle No. of the cell shown in Fig. 23.

There were no significant changes in the voltage profiles from cycle to cycle. The fairly steady cathode utilization indicates the good rechargeability of the stoichiometric oxide. Indeed, the cycling of a hermetically sealed cell, to be discussed later, indicated practically no change in capacity from the first to the 80th cycle.

In the stoichiometric oxide the maximum capacity of 0.66 e^-/V appears just at the transition stage of the semiconducting to the insulating phases of the $Li_xV_6O_{13}$ ternary. Thus, the electrical isolation of the insulating $Li_xV_6O_{13}$ phases which occurs in the cycling of the non-stoichiometric oxide probably does not happen in the stoichiometric oxide electrode.

Two other cells utilizing the stoichiometric oxides but with higher cathode loading capacities were also cycled.

In cell #280-075, the cathode (70 w/o V_6O_{13}, 20 w/o C, 10 w/o Teflon, 73 mil thick) had a capacity density of 30·5 mAh/cm^2. The data are given in Table 12. In the first six cycles the discharge current densities* were varied between 8.0 and 0.5 mA/cm^2. The capacity in the 4th cycle at 2 mA/cm^2, after the prior high rate discharges, was 0.57 e^-/V, indicating that the high rate discharges did not affect the reversibility of the cathode. Beginning with the seventh cycle, the cell was cycled at current densities of 2 mA/cm^2 for discharge and 1 mA/cm^2 for charge. The cathode utilization in the seventh discharge was 0.52 e^-/V. With continued cycling at these rates the capacity gradually decreased. At the 22nd charge, the charge current density was reduced to 0.50 mA/cm^2; this resulted in an increase in the cathode rechargeability by 25% compared to the previous charge. This suggests that one of the reasons for the decreasing cathode utilization in cycles 7-22 was the rate of charging which was probably higher than the optimum required for good rechargeability. Beginning with the 23rd discharge, the cell was cycled at current densities of 1.0 mA/cm^2 for discharge and 0.5 mA/cm^2 for charge. The cathode utilization was 0.5 e^-/V in the 23rd discharge and 0.46 e^-/V in the 24th discharge.

Cell #280-074 utilizing a 20.8 mAh cathode (51 mil thick) was also cycled with high initial discharge rates. The behavior is identical to that of the previous cell. Beginning with the seventh cycle, the current densities were 2 mA/cm^2 for both discharge and charge. The data are tabulated in Table 13. The cathode utilization in the seventh discharge at 2 mA/cm^2 was 0.54 e^-/V. However, the seventh recharge at 2 mA/cm^2 corresponded to only 79% of the discharge. This is in contrast to the 98% rechargeability in cell #280-075, where, in the seventh charge, the current density was 1.0 mA/cm^2. It appears that although the vanadium oxide can be discharged at high rates, the charge rate should be maintained fairly low, preferably <1.0 mA/cm^2, to obtain good cathode rechargeability.

*This was the same cell used in the rate studies. (see Fig. 19)

Table 12

Cycling Data for Li/V_6O_{13} Cell No. 280-075

Cathode: Stoichiometric V_6O_{13} (30.5 mAh/cm^2, 73 mil thick), 20 w/o carbon, 10 w/o Teflon. Area = 15.5 cm^2 for both sides.

Electrolyte: 2Me-THF, 1.5M $LiAsF_6$

Cycle Number	Discharge Current Density mA/cm^2	Discharge Capacity		Charge Current Density mA/cm^2	Charge Capacity	
		mAh	$\bar{e}/V$		mAh	% of Discharge
1	8	50	0.11	0.5	50	100
2	6	108	0.24	0.5	108	100
3	4	204	0.44	0.5	202	99
4	2	259	0.57	0.5	257	99
5	1	268	0.59	0.5	266	99
6	0.5	287	0.63	0.5	285	99
7	2	238	0.52	1.0	232	97
8	2	223	0.49	1.0	220	99
9	2	212	0.46	1.0	208	98
10	2	204	0.45	1.0	200	98
11	2	200	0.44	1.0	200	100
12	2	203	0.44	1.0	200	99
13	2	195	0.43	1.0	190	98
14	2	189	0.42	1.0	186	98
15	2	184	0.40	1.0	180	98
16	2	178	0.39	1.0	176	99
17	2	173	0.38	1.0	170	98
18	2	171	0.37	1.0	169	99
19	2	171	0.37	1.0	168	99
20	2	170	0.37	1.0	168	99
21	2	167	0.36	1.0	165	99
22	2	166	0.36	0.5	206	124
23	1.0	228	0.50	0.5	220	96
24	1.0	209	0.46	0.5	206	98
25	1.0	201	0.44	0.5	200	99

Table 13

Cycling Data for Li/V_6O_{13} Cell No. 230-074

Cathode: Stoichiometric V_6O_{13} (20.8 mAh/cm^2, 51 mil thick), 20 w/o carbon, 10 w/o Teflon. Area = 15.5 cm^2 for both sides.

Electrolyte: 2Me-THF/1.5M $LiAsF_6$

Cycle Number	Discharge Current Density mA/cm^2	Discharge Capacity		Charge Current Density mA/cm^2	Charge Capacity	
		mAh	$\bar{e}$/V		mAh	% of Discharge
1	8	53	0.17	0.5	44	83
2	6	76	0.24	0.5	79	104
3	4	150	0.48	0.5	144	96
4	2	187	0.60	0.5	176	94
5	1	180	0.58	0.5	180	100
6	0.5	186	0.60	0.5	186	100
7	2.0	169	0.54	2.0	133	78
8	2.0	132	0.42	2.0	122	93
9	2.0	121	0.39	2.0	121	100
10	2.0	119	0.38	2.0	113	95
11	2.0	108	0.35	2.0	102	94
12	2.0	103	0.33	2.0	101	97
13	2.0	99	0.32	2.0	93	94
14	2.0	93	0.30	2.0	97	104
15	2.0	96	0.31	2.0	88	92
16	2.0	88	0.28	2.0	88	100
17	2.0	88	0.28	2.0	96	108
18	2.0	91	0.29	2.0	84	91
19	2.0	86	0.27	2.0	86	100
20	2.0	82	0.26	2.0	82	100
21	2.0	79	0.25	2.0	81	102
22	2.0	78	0.25	2.0	80	101
23	2.0	78	0.25	2.0	78	100
24	2.0	76	0.24	2.0	76	100
25	2.0	76	0.24	2.0	76	100
26	1.0	95	0.31	0.5	142	150
27	1.0	146	0.47	0.5	137	95
28	1.0	134	0.43	0.5	125	93
29	1.0	136	0.44	0.5	133	97
35	1.0	135	0.43	0.5	130	96

This drawback may be eliminated with improved cathode fabrication. At the 26th cycle, the current densities were reduced to 1.0 mA/cm^2 for discharge and 0.5 mA/cm^2 for charge. The cathode utilization increased to 0.47 e^-/V at the 27th discharge. The increased cathode capacity again resulted from the improved recharge at 0.5 mA/cm^2 in the 26th charge. This cell was cycled 36 times and the capacity in the 36th discharge was 0.42 e^-/V.

3.5.3 Morphology of Extensively Cycled Oxides

The SEM photographs of extensively cycled stoichiometric and non-stoichiometric oxide cathodes are shown in Figures 26 and 27 respectively. The stoichiometric oxide retains its crystallinity even after extensive cycling. It appears, however, that the crystals have lost their original prismatic shapes and have become rectangular slabs.

The non-stoichiometric oxide also appears to have undergone some changes in crystallinity with cycling. The material which did not reveal any apparent crystallinity in the SEM before cycling appears to contain a few rectangular crystals after cycling. The higher degree of crystallinity may have resulted from the dynamics of Li incorporation into and expulsion from the oxide lattice.

Fig. 26. The SEM of cycled stoichiometric oxide Magnification, 1000X.

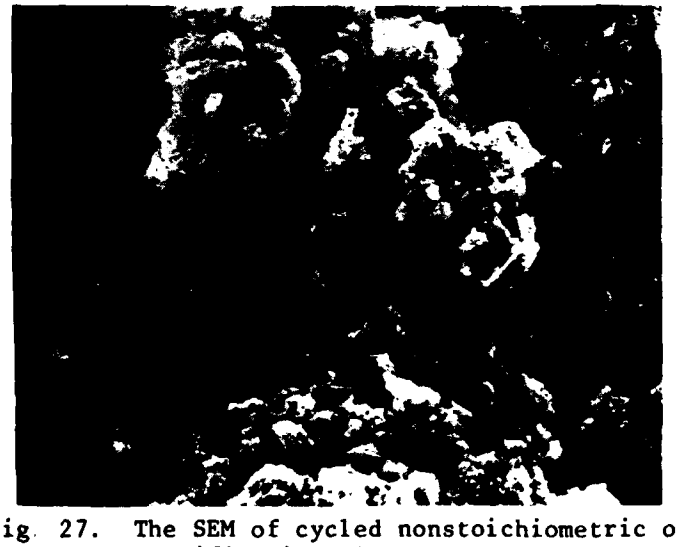

Fig. 27. The SEM of cycled nonstoichiometric oxide. Magnification, 1000X

4. CONSTRUCTION AND TESTING OF HERMETICALLY SEALED CELLS

Three types of hermetically sealed cells were constructed and tested. These were: i) hermetic laboratory test cells. These cells were designed to provide a suitable test vehicle for extended cycling studies avoiding the deleterious electrode structural problems on cell cycle life. (ii) hermetic spirally wound cells. These cells were constructed to understand the problems of spiral geometry on the cycle life of both the Li and oxide electrodes, aiding in the development of advanced cells; (iii) high capacity prismatic cells. These cells were aimed at assessing the effects of scale-up on cathode and anode utilizations and on overall cell-cycle life.

4.1 Hermetically Sealed Laboratory Test Cells

The basic configuration of the electrode package consists of an alternating stack of lithium and cathode electrodes. Each electrode is enclosed in a heat-sealed porous polypropylene membrane (Celgard 2400 Series) bag. The end lithium electrodes have single sided laminations whereas the center electrodes have double sided laminations. The overall thickness of the pack is roughly 150 $\pm$ 10 mil. The electrode leads projecting from the top of the pack are aligned such that all anode leads are on one side and all cathode leads are on the other side. The anode and cathode leads are spot welded together among their types to form singular lead tabs. A D-size cell can is used for packaging the electrode stack. A polyethylene disk 1.250" dia x 0.005" thick is placed in the bottom of the Ni plated cold rolled can for electrical insulation. The electrode package is sandwiched between two Teflon hemi-cylinders and this assembly is inserted into the can with both electrode leads projecting upward. A stainless steel shim is wedged between one hemi-cylinder and the inside wall of the can such that maximum compression is applied to the electrode pack by the spring action of the shim. The electrode leads are then spot welded to the tab connections on the cover assembly. With leads attached, the cover is pressed into the can and spot welded to the can to insure that the lip of the cover will remain flush with the can lip for TIG weld sealing. Electrolyte is introduced into the cell by vacuum filling. A schematic of the sealed cell is shown in Fig. 28.

Cell No. 314-21-03 utilized stoichiometric V_6O_{13}. The cathode contained 70 w/o V_6O_{13}, 20 w/o C and 10 w/o Teflon. The cell had a cathode area of 39 cm^2. The cell was cycled between 3.0V and 1.9V. A plot of cathode utilization vs. cycle number is shown in Fig. 29. Some typical cycles are shown in Fig. 30. The cell exhibited excellent cycling

[1] Two of these cells have been sent to ET and D Laboratory for their evaluation.

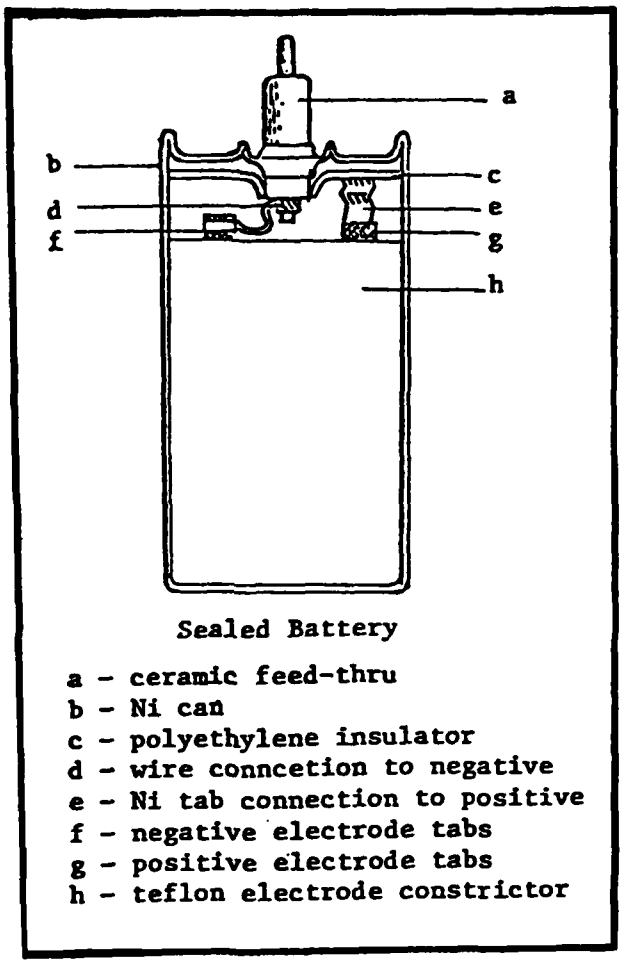

Fig. 28. Schematic view of sealed Li/V_6O_{13}, laboratory test cell.

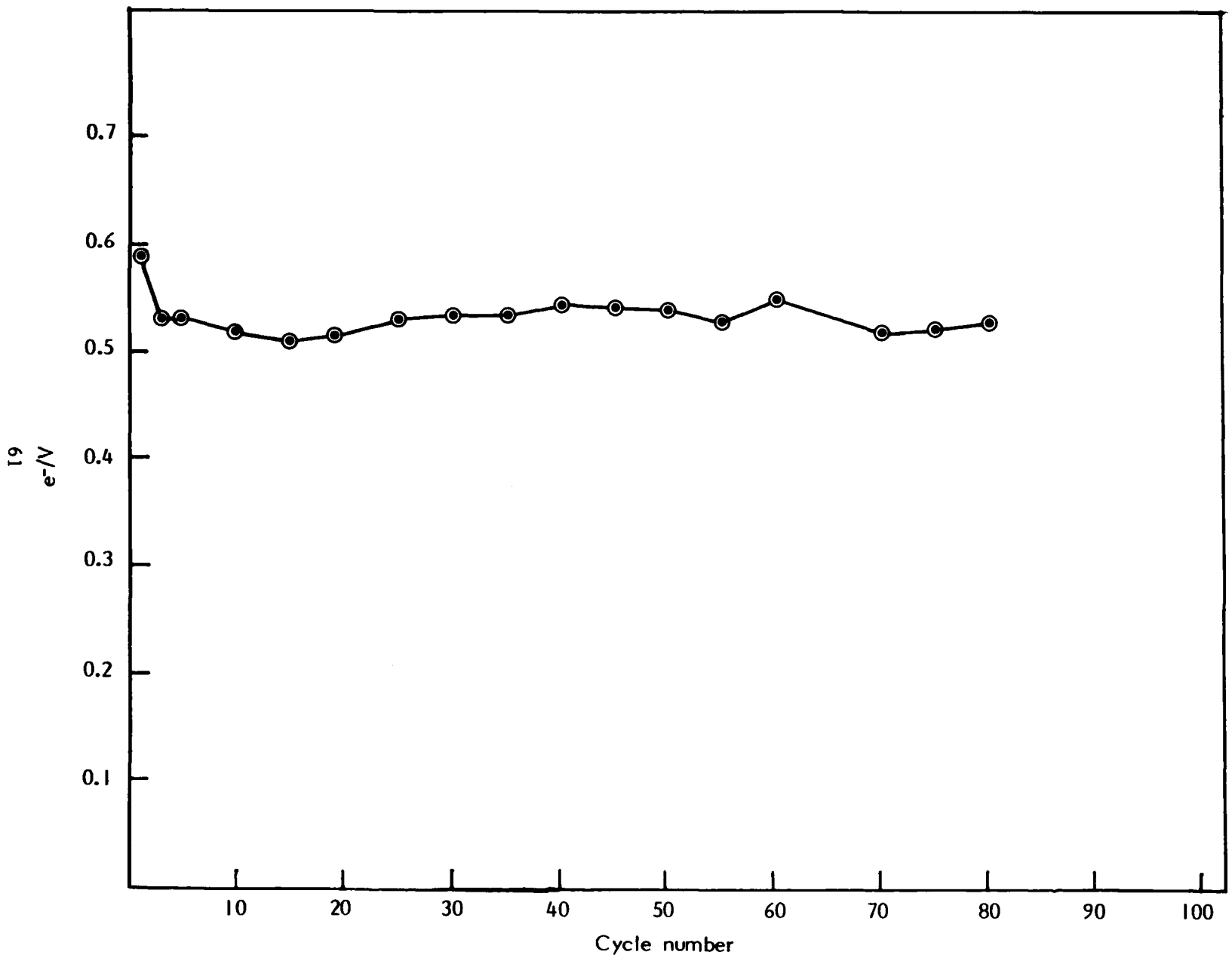

Fig. 29. Cathode utilization versus cycle number for laboratory test Cell 314-21-03 utilizing stoichiometric V_6O_{13}.

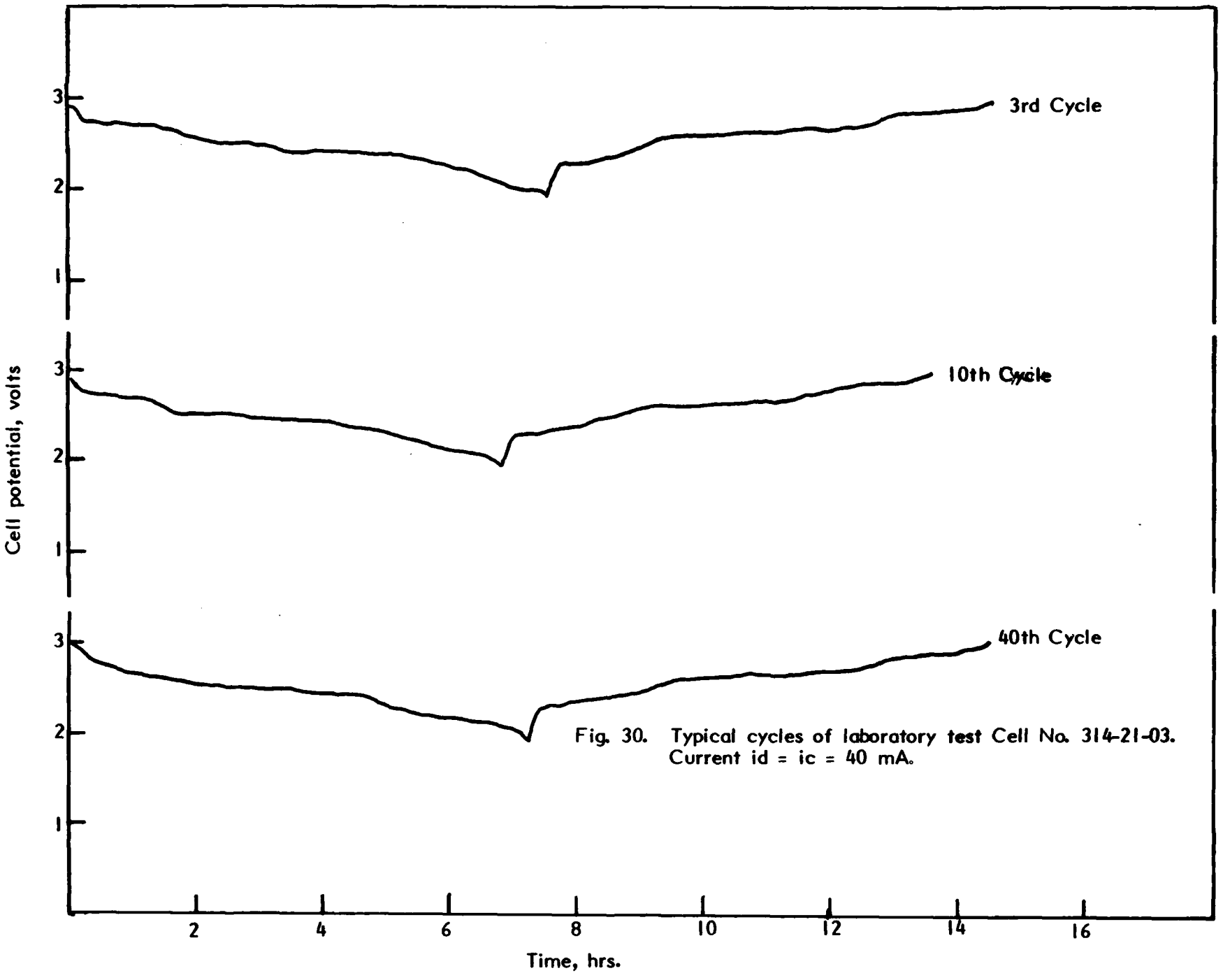

Fig. 30. Typical cycles of laboratory test Cell No. 314-21-03. Current id = ic = 40 mA.

behavior. The first cycle was performed at 20 mA (0.5 mA/cm^2). The cathode utilization was 0.59 e$^-$/V, nearly close to the theoretical value, and the recharge efficiency was 96%. Beginning with the 2nd cycle, the current was set at 40 mA (1.0 mA/cm^2) for both discharge and charge. The cathode utilization remained practically the same through 80 cycles*.

Cycling of this cell has demonstrated the excellent reversibility of the stoichiometric V_6O_{13} within the cycling limits of 3.0 and 1.9V. The data have also shown the importance of having a proper test vehicle for evaluating the rechargeability of high capacity lithium intercalation cathodes. An aspect of particular importance is to minimize the deleterious effects on utilization of electrode structural problems such as swelling during cycling. These were minimal in the present case.

4.2 Hermetically Sealed, Spirally Wound Cell

A cell approximately of the AA size was constructed in a Ni plated steel can. The cell specifications are shown below. The vanadium oxide was non-stoichiometric V_6O_{13}.

Cell Can: Ni plated steel can; 1.5" height, 5/8" OD.

Cathode: 55 w/o V_6O_{13}, 35 w/o graphite, 10 w/o Teflon, pasted on Ni Exmet (5Ni5-5/o). Cathode capacity, 375 mAh based on 1e$^-$/V. The pasted electrode was 2.5 cm wide, 7.5 cm long and 1 mm thick. The oxide was non-stoichiometric V_6O_{13}.

Anode: Li foil pressed onto Ni Exmet (5Ni-5-5/o). Anode capacity, 940 mAh. Total area of Li facing cathode, 38 cm^2.

Separator: Double wrap polypropylene (Celgard 2400), 1 mil thick.

Electrolyte: 1.5M $LiAsF_6$/2Me-THF, ~3.5 ml.

The cell was cycled between voltage limits of 3.0V and 1.9V. The current was varied during various stages of cycling. The results are shown in Fig. 31, plotted as cathode utilization versus cycle number. Typical cycles are shown in Fig. 32.

The first 18 cycles were performed at 40 mA (1 mA/cm^2). The capacity in the first discharge corresponded to 0.53 e$^-$/V. In laboratory cells utilizing this cathode material, capacities, usually, of 0.9 to 1.0 e$^-$/V are obtained at 1.0 mA/cm^2. In the first charge only 60% of the discharge capacity was recharged. The capacity loss in the first

*At the writing of the Final Report, cycling of this cell was continuing. Complete data will be reported in related publications.

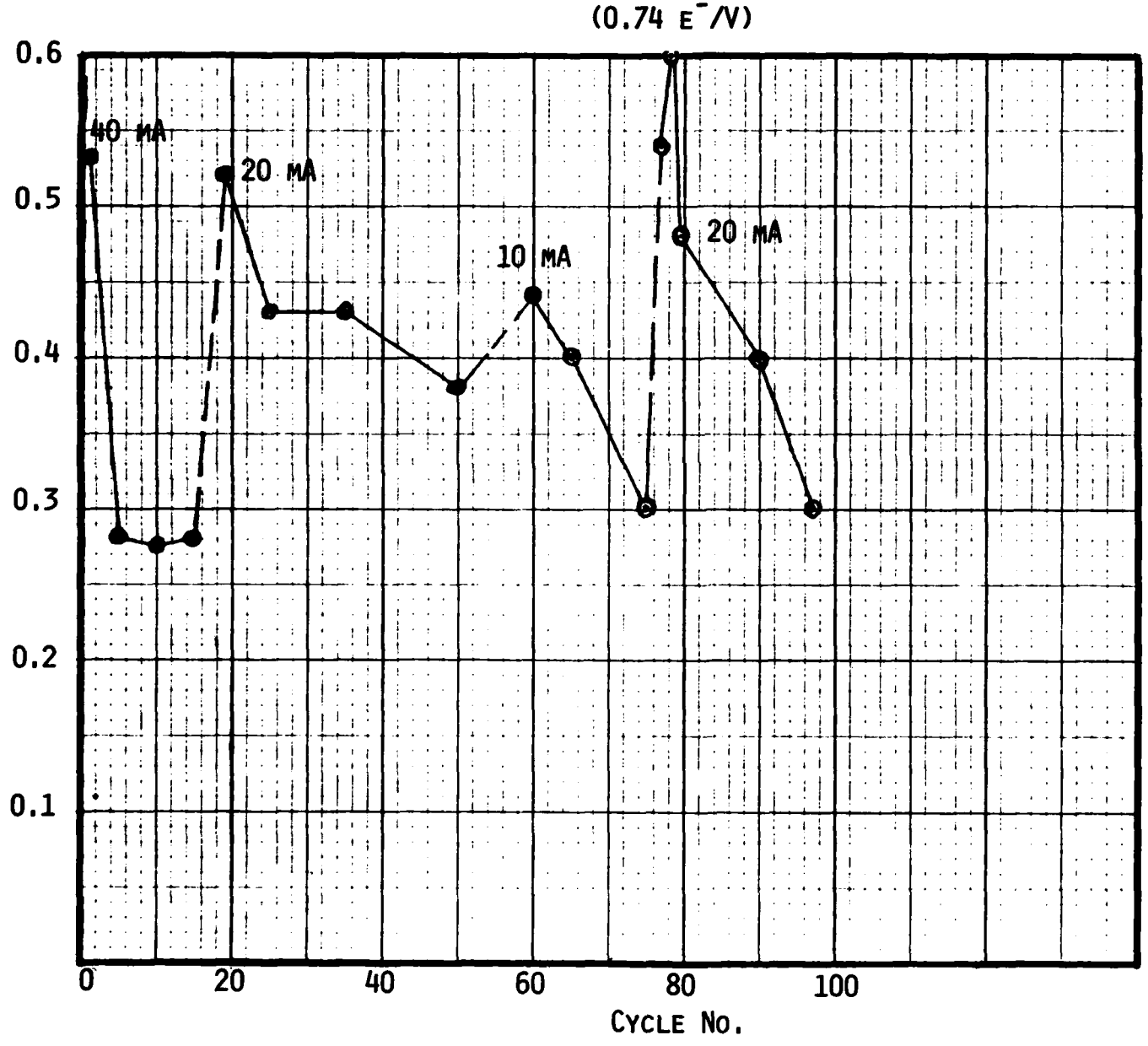

Fig. 31. Cathode utilization versus cycle number of spirally wound Li/V_6O_{13} cell.

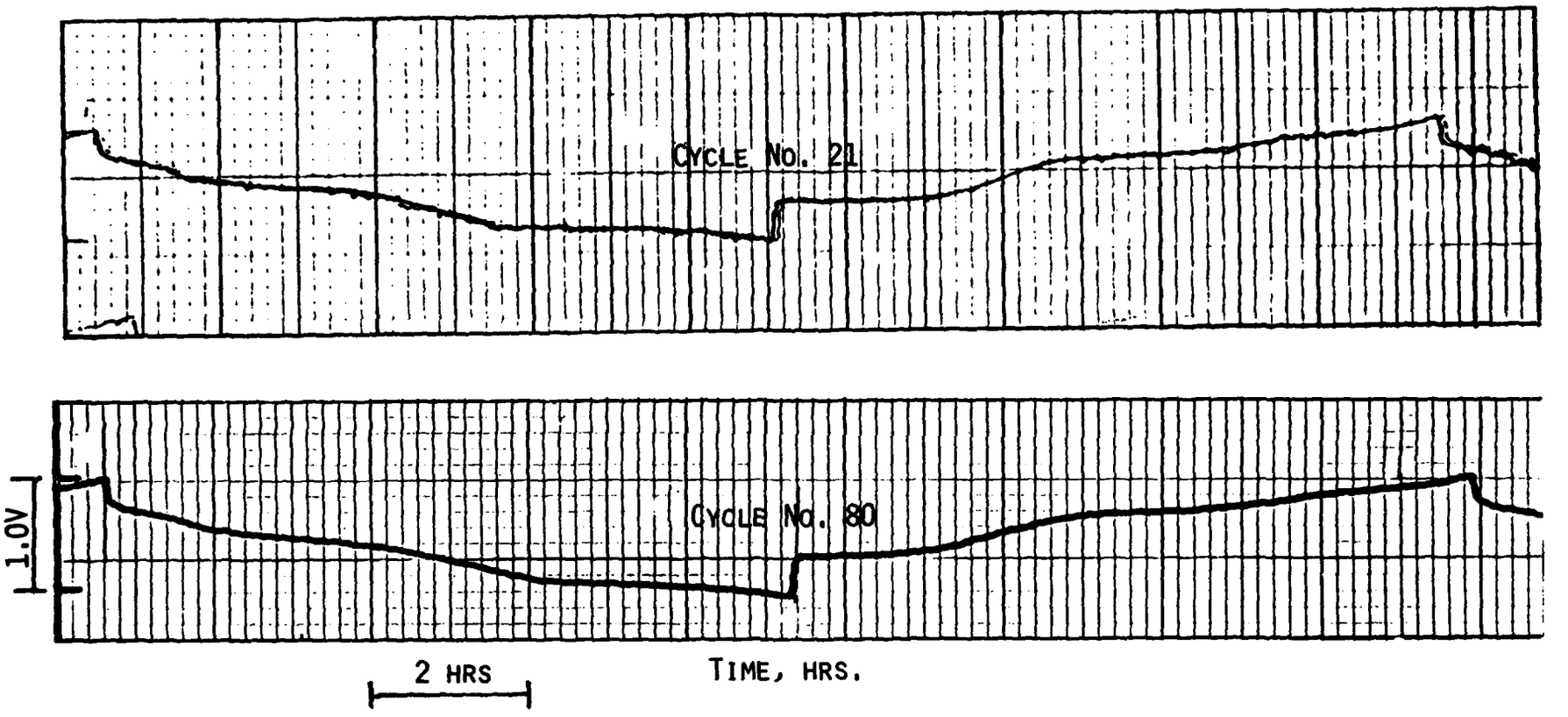

Fig. 32. The 21st and 80th cycles of spirally wound Li/V_6O_{13} cell. Current = 20 mA.

charge is ∿20% more than what is normally found in laboratory cells. The capacity in the second discharge was 0.30 e^-/V. The cathode utilization was maintained at an average value of 0.27 e^-/V until the 18th discharge. The current was reduced to 20 mA (0.5 mA/cm^2) at the 18th charge. The rechargeability improved substantially. The capacity in the 19th discharge corresponded to 0.5 e^-/V, a portion of which involved utilization of cathode material unused in earlier cycling. From the 18th charge until the 59th discharge, the current was maintained at 20 mA (0.5 mA/cm^2). The cell capacity showed a declining trend at about 0.75% loss per cycle. The capacity at the 59th discharge was 0.35 e^-/V. At the 60th discharge the current was reduced to 10 mA which made the utilization increase to 0.44 e^-/V. There was no change in capacity until the 65th discharge when the current was again increased to 20 mA. The increased current caused the capacity to decline in subsequent cycles. At the 77th discharge, the current was reduced to 2 mA (0.05 mA/cm^2). The capacity increased to 0.54 e^-/V. In the 77th charge, again performed at 2 mA, the rechargeability improved substantially so that a capacity of 0.74 e^-/V was obtained in the 78th discharge at 2 mA. In the 79th discharge the current was raised back to 20 mA. The cathode utilization at 20 mA now was much larger than before the low rate charging. The test was continued until the 95th discharge. The Li remaining now in the cell was stripped off by discharging the cell to 0.0V. The Li electrode efficiency was calculated from the total amounts of charge put in and charge taken out in the 95 cycles. This was found to be 96.5%, in good agreement with the thin plate cycling efficiency reported for Li in this electrolyte by Koch (11).

Cycling of this cell has demonstrated the following: 1) the Li electrode exhibits high cycling efficiency in a complete cell demonstrating the excellent compatibilities of the cell components at ambient temperature, 2) Li can be cycled in a spiral configuration with high charge densities without encountering short-circuiting.

The rate capability of the cell was not good. However, this could be improved with further optimization.

4.3 High Capacity Prismatic Cells

The cell contains a stack of rectangular electrodes. Specifically, the cell can consists of deep drawn stainless steel (SS316) with the following dimensions:

Width	5.766 cm	2.270 in
Depth	1.968 cm	0.775 in
Height	5.588 cm	2.200 in
Wall Thickness:	0.056 cm	0.022 in

The cover contains two glass to metal compression seals. The cell specifications were as follows:

Cathode: 16.1 non-stoichiometric oxide (70 w/o), 20 w/o C and 10 w/o Teflon. Theoretical cathode capacity, 5 Ah (1 e^-/V). The cell has seven cathodes; each cathode is 5·0 cm x 3.75 cm per side, total area, 265 cm^2.

Anode: 5.18g Li (20 Ah). The cell has eight anodes; each is 5 cm x 3.75 cm. Total area is 265 cm^2.

Separator: Celgard 2400, double wrap.

Electrolyte: 18-22g, 2Me-THF, 1.5M $LiAsF_6$.

Cell Weight: 115g (about half of this weight is due to cell can and cover).

Four of these cells[1] were built on the present contract. Data for the first cycles of these cells at 140 mA (0.5 mA/cm^2) are shown in Table 14. Typical first cycles of two of these cells are shown in Figure 33.

All the cells exhibited practically identical behavior. The capacities in the first discharge exceeded 5 Ah (1 e^-/V). In the first charge ∿20% of the capacity was not recharged. These characteristics are identical to those observed in small laboratory cells utilizing this oxide.

Cells 314-32-01 and 314-32-03 were further cycled[2]. Data for cell 314-32-03 are listed in Table 15. Some typical cycles are shown in Figure 34. The cell has exhibited fairly consistent cycling behavior since the second cycle. The cell capacity in the 9th discharge was 3.45 Ah, which is 87% of the capacity in the 2nd discharge. The overall performance of this high capacity cell is somewhat superior to that observed in small laboratory cells utilizing non-stoichiometric V_6O_{13}.

With a cell weight of 115g and a mid-discharge voltage of 2.3V, the measured 5.3 Ah capacity in the first discharge translates to an energy density of 106 Whr/kg (48 Whr/lb). The external volume of the cell is ∿64 cm^3, resulting in a volumetric energy density of 190 Whr/dm^3.

---

[1] Two of these cells have been sent to Eradcom for evaluation. The cells were 314-32-02 and 314-32-04. They are sent after cycling once.

[2] At the writing of this report, cycling of these cells is still in progress. Therefore only partial data are given here.

Table 14

Cycling Data for Prismatic Li/V_6O_{13} Cells

Cell No.	Current mA	Capacity[2] in the first discharge Ah	Capacity[3] in the first charge Ah
314-32-01	140	5.18	4.0
314-32-02	140	5.21	4.39
314-32-03	140	5.04	4.10
314-32-04	140	5.38	4.33

[2] to 1.9V
[3] to 3.0V

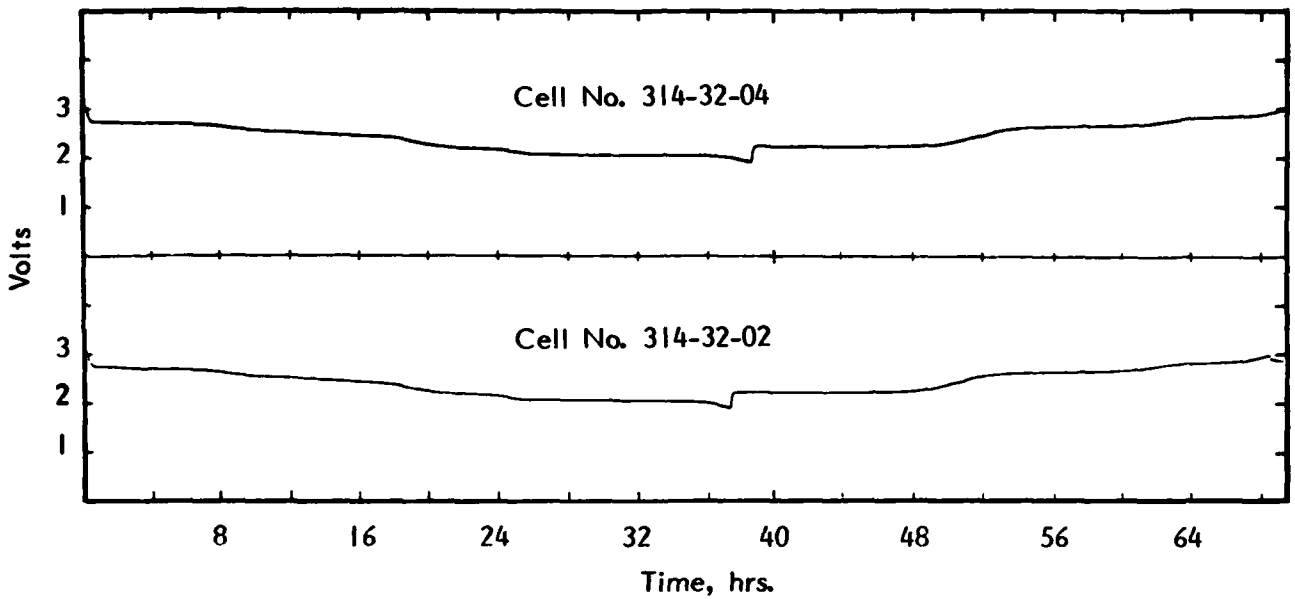

Fig. 33. The first cycles of the prismatic cells. Voltage limits, 3.0 and 1.9. Current = 140 mA. These cells were sent to ERADCOM for further evaluation.

Table 15

Cycling Data for Prismatic Li/V_6O_{13} Cell No. 314-32-03

	Discharge		Charge	
Cycle No.	Current, mA	Capacity	Current, mA	Capacity (Ah)
1	140	5.04	140	4.17
2	-	-	-	-
3	140	4.07	140	4.12
4	300	3.81	200	3.73
5	↓	3.80	↓	3.74
6		3.66		3.58
7		3.57		3.56
8		3.63		3.62
9		3.45		3.68
10		3.66		3.60
11		3.63		3.58
12		3.54		3.54
13		3.54		3.52
14		3.57		3.54
15		3.57		3.54
16		3.51		3.52
17		3.57		3.52
18		-		-
19		-		-
20		3.51		3.44

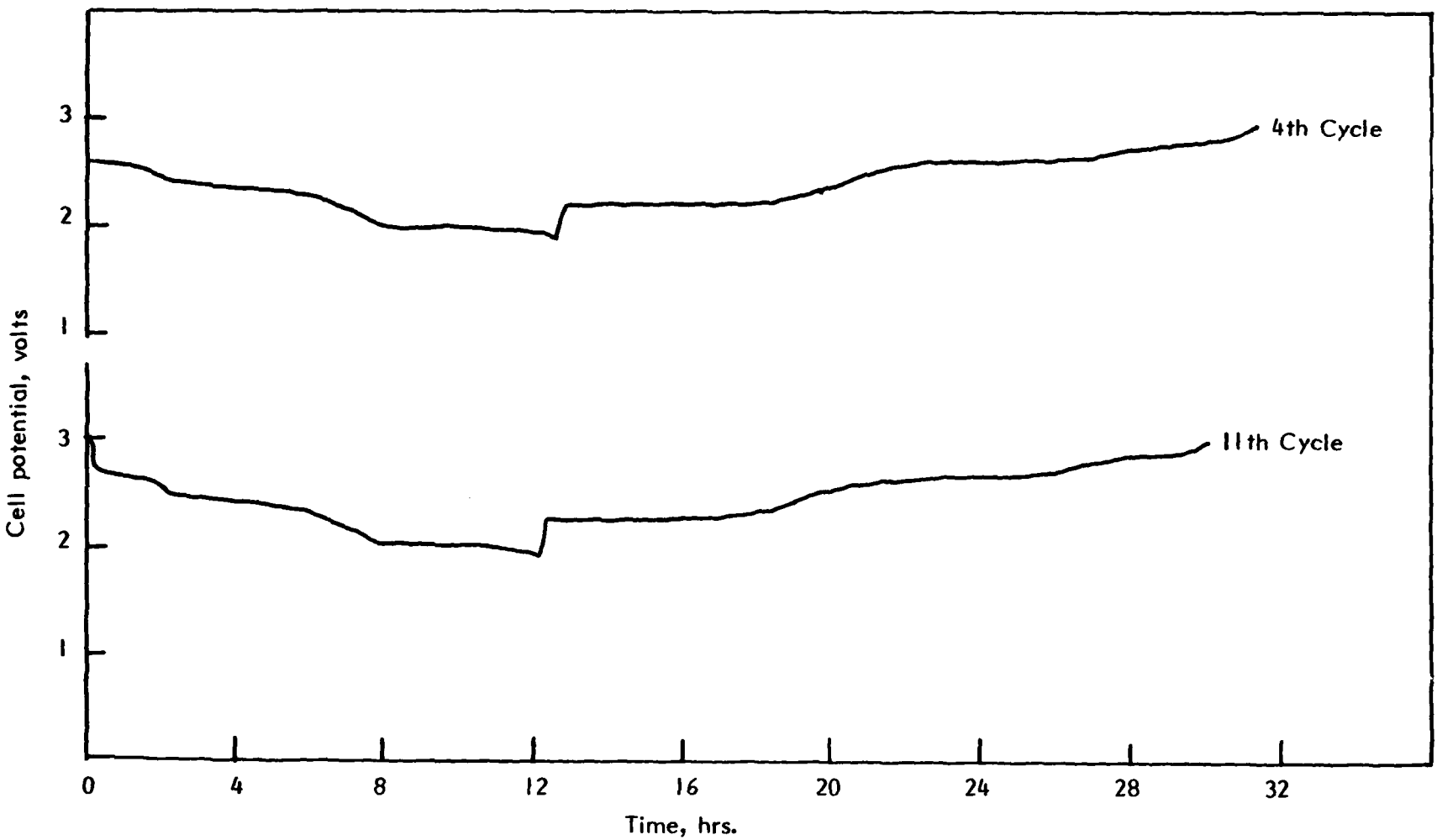

Fig. 34. The 4th and 11th cycles of prismatic Cell No. 314-32-013. Current id = 300 mA; ic = 200 mA.

5. SUMMARY AND CONCLUSIONS

Two forms of the vanadium oxide, V_6O_{13}, were synthesized and characterized. These were a stoichiometric form, i.e., $VO_{2.17}$ and a slightly non-stoichiometric form, i.e., $VO_{2.19}$.

Stoichiometric V_6O_{13} was prepared by heating requisite quantities of V_2O_5 and V powder for 24 hrs. at 650°C. It was characterized by X-ray and SEM data. SEM analysis revealed this oxide to be a highly crystalline material composed of 4-5 μm wide and 14-18 μm long crystallites. For a cathode having a theoretical capacity density of 20 mAh/cm^2 (based on 1 e^-/V), the utilization in the early cycles was ∿0.6 e^-/V at current densities of 0.5, 1.0 and 2.0 mA/cm^2 and 0.45 e^-/V at 4 mA/cm^2. Rate-capacity behavior similar to these was exhibited also by cathodes having capacity densities of 10 mAh and 30 mAh per cm^2. The discharge to 1.9V proceeded in four distinct voltage regions with a mid-discharge potential of ∿2.3V. The cathode exhibited good rechargeability. One cell was cycled 80 times with a steady cathode utilization of 0.52 e^-/V.

The slightly non-stoichiometric V_6O_{13}, was prepared by the thermal decomposition of NH_4VO_3 at 450°C. X-ray diffraction pattern of this material was virtually identical to that of stoichiometric V_6O_{13}. However, SEM data revealed it to be composed of much smaller particles with very little apparent crystallinity. First discharge of the material resulted in a higher capacity than the stoichiometric oxide. For example, capacities between 0.90 and 1.0 e^-/V were obtained at current densities between 0.50 and 2.0 mA/cm^2. The extra capacity results in a plateau at ∿2.1V. In the first charge, a loss in capacity amounting to 15-20% of the first discharge occurs. This loss is independent of charge current densities between 0.1 and 2.0 mA/cm^2. With continued cycling, a gradual loss in cathode utilization occurs in the early cycles. After 15 cycles or so, the cathode utilization becomes steady at ∿0.60 e^-/V.

The discharge characteristics of the stoichiometric oxide at 60°C were similar to that of the non-stoichiometric oxide at room temperature.

The rechargeability of both the oxides were found to be sensitive to the lower voltage cutoff. The most safe voltage limits of cycling were 3.0 and 1.9. Potentiostatic discharges of the oxides as a function of voltages between 1.9 and 1.3 revealed a high capacity irreversible reduction process at ∿1.6V.

Three types of hermetically sealed cells were contructed and tested. In a high capacity (5Ah) prismatic cell utilizing the non-stoichiometric oxide energy densities of 106 Whr/kg and 190 Whr/DM^3 were achieved in the first cycle. These energy densities were, however, reduced by 15-20% in the second discharge.

With the highly reversible stoichiometric oxide, based on the present cell design, the energy densities would be ∿60 Whr/kg and 115 Whr/DM^3.

The two major factors limiting the volumetric energy densities are the amount of carbon required for fabricating an acceptable cathode and the amount of Li required to achieve a specified number of cycles. Considerable improvements in volumetric energy density may be possible by the use of metallic conductive additives to the V_6O_{13} and by improvements in the Li cycling efficiency.

6. REFERENCES

1. S. B. Brummer, K. M. Abraham, V. R. Koch and G. L. Holleck, Final Report, Contract 4503510 to Lawrence Berkely Laboratory by EIC Laboratories, Inc., August 1980.

2. V. R. Koch, Ibid., Chapter II.

3. V. R. Koch and J. H. Young, Science, 204, 499 (1979).

4. M. S. Whittingham, Science, 192, 1126 (1976).

5. G. L. Holleck, K. M. Abraham and S. B. Brummer in Proceedings of the symposium on "Power Sources for Biomedical Implantable Applications; Ambient Temperature Lithium Batteries," B. B. Owens and N. Margalit, eds., The Electrochemical Society, PV80-4, 1980.

6. K. M. Abraham in Chapter III, Final Report, Contract 4503510 to Lawrence Berkely Laboratory by EIC Laboratories, Inc., August 1980.

7. D. W. Murphy and P. A. Christian, Science, 205, 65 (1979).

8. D. W. Murphy, P. A. Christian, F. J. Disalvo and J. W. Carides, J. Electrochem. Soc., 126, 497 (1979).

9. K. Wilhelmi, K. Waltersson and L. Kihlborg, Acta. Chem. Scandinavia, 25, 2675 (1971).

10. V. R. Koch and J. H. Young, J. Electrochem. Soc., 125, 1371 (1978).

11. J. L. Goldman, R. M. Mank, J. H. Young and V. R. Koch, J. Electrochem. Soc., 127, 1461 (1980).

12. C. R. Walk and J. S. Grove, J. Electrochem. Soc., 122, 68C (1975).

13. K. M. Abraham, Unpublished results.

DISTRIBUTION LIST

Defense Technical Information Center (12)
Attn: DTIC-TCA
Cameron Station (Bldg. 5)
Alexandria, VA 22314

GIDEP Engineering & Support Dept. (1)
TE Section
P. O. Box 398
Norco, CA 91760

Director (1)
Naval Research Laboratory
Attn: Code 2627
Washington, D. C. 20375

Rome Air Development Center (1)
Attn: Documents Library (TILD)
Griffiss AFB, NY 13441

Deputy for Science & Technology (1)
Office, Asst. Sec. Army (R&D)
Washington, D. C. 20310

HQDA (DAMA-ARZ-D/ (1)
Dr. F. D. Verderame)
Washington, D. C. 20310

Director (1)
U.S. Army Materiel Systems Analysis Actv.
Attn: DRXSY-T
Aberdeen Proving Ground, MD 21005

Commander, DARCOM (1)
Attn: DRCDE
5001 Eisenhower Avenue
Alexandria, VA 22333

Cdr, U.S. Army Signals Warfare Lab (1)
Attn: DELSW-OS
Vint Hill Farms Station
Warrenton, VA 22186

Cdr, PM Concept Analysis Ctrs (1)
Attn: DRCPM-CAC
Arlington Hall Station
Arlington, VA 22212

Cdr, Night Vision & Electro-Optics (1)
ERADCOM
Attn: DELNV-D
Fort Belvoir, VA 22060

Cdr, Atmospheric Sciences Lab (1)
ERADCOM
Attn: DELAS-SY-S
White Sands Missile Range, NM 88002

Cdr, Harry Diamond Laboratories (1)
Attn: DELHD-CO, TD (In Turn)
2800 Powder Mill Road
Adelphi, MD 20783

Cdr, ERADCOM (1)
Attn: DRDEL-CG, CD, CS (In Turn)
2800 Powder Mill Road
Adelphi, MD 20783

Cdr, ERADCOM (1)
Attn: DRDEL-CT
2800 Powder Mill Road
Adelphi, MD 20783

Commander
U.S. Army Electronics R&D Command
Fort Monmouth, NJ 07703

DELET-P (1)
DELEW-D (1)
DELET-DD (1)
DELSD-L (Tech Library) (1)
DELSD-L-S (STINFO) (2)
Originating Office
DELET-PR (Hunger) (22)

Commander (1)
U.S. Army Communications R&D Command
Attn: USMC-LNO
Fort Monmouth, NJ 07703

Advisory Group on Electron Devices (2)
201 Varick Street, 9th Floor
New York, NY 10014

CMDR, MICOM (1)
Attn: DRCPM-HDE
Redstone Arsenal, AL 35809

Transportation Systems Center (1)
Kendall Square
Cambridge, MA 02142
Attn: Dr. Normal Rosenberg

Foote Mineral Company (1)
Route 100
Exton, PA 19341
Attn: Dr. H. Grady

Honeywell, Inc. (1)
104 Rock Road
Horsham, PA 19044

Sanders Associates, Inc. (1)
Sonobuoy Division
95 Canal Street
Nashua, NH 03060

Eagle-Picher Industries, Inc. (1)
Electronics Division
P. O. Box 47
Joplin, MO 64801
Attn: Mr. Robert L. Higgins

Yardney Electric Company (1)
82 Mechanic Street
Pawcatuck, CT 06379
Attn: Technical Library

P. R. Mallory & Company, Inc. (1)
Northwest Industrial Park
Burlington, MA 01803
Attn: Dr. A. N. Dey

Exxon Research & Engg. Company (1)
Corporate Research Laboratory
Linden, NJ 07036
Attn: Dr. R. Hamlen

Argonne National Laboratories (1)
9700 South Cass Avenue
Argonne, IL 60439
Attn: Dr. E. C. Gay

GTE Sylvania, Inc. (1)
77 A Street
Needham Heights, MA 02194
Attn: Mr. Richard Pabst

Tufts University (1)
Department of Chemistry
Medford, MA 02155

General Motors Corporation (1)
Research Laboratories
General Motors Tech. Center
12 Mile and Mounds Roads
Warren, MI 48090

Union Carbide Corporation (1)
Parma Research Center
P. O. Box 6116
Cleveland, OH 44101

P. R. Mallory & Company, Inc. (1)
S. Broadway
Tarrytown, NY 10591
Attn: J. Dalfonso

North American Rockwell Corp. (1)
Atomics Internation Division
P. O. Box 309
Canoga Park, CA 91304
Attn: Dr. L. Heredy

General Electric Research & (1)
Development Center
P. O. Box 8
Schenectady, NY 12301
Attn: Dr. Stefan Mitoff

University of California (1)
Department of Science & Research
Santa Barbara, CA 93100
Attn: Dr. J. Kennedy

Gulton Industries, Inc. (1)
Metuchen, NJ 08840
Attn: Mr. S. Charlip

INCO Research & Development Ctr (1)
Sterling Forest
Suffern, NY 10901
Attn: Nehemiah Margalit

Director (1)
Propulsion and Power Division
Mail Code EP5
NASA-Johnson Space Center
Houston, TX 77058
Attn: Mr. B. J. Bragg

GTE Laboratories, Inc. (1)
520 Winter Street
Waltham, MA 02154
Attn: Dr. Ronald McDonald

Electrochimica (1)
2485 Charleston Road
Mountain View, CA 94040
Attn: Dr. Eisenberg

Dr. Hugh Barger (1)
P. O. Box 2232
Davidson, NC 28036

Energy Storage & Conversion Dept. (1)
TRW Systems
One Space Park
Redondo Beach, CA 90278
Attn: Dr. H. P. Silverman

Sanders Associates, Inc. (1)
24 Simon Street
Mail Stop NSI-2208
Nashua, NH 03060
Attn: J. Marshall

Power Conversion, Inc. (1)
70 MacQuesten Parkway
Mount Vernon, NY 10550
Attn: Stuart Chodosh

Portfolio Manager (1)
Hooker Chemicals & Plastics Corp.
M.P.O. Box 8
Niagara Falls, NY 14302

G207 (1)
S.R.I.
Menlo Park, CA 94025
Attn: Dr. Leonard Nanis

Bell Laboratories (1)
600 Mountain Avenue
Murray Hill, NJ 07974
Attn: Dr. J. J. Auborn
Room 1A-317

Stonehart Associates, Inc. (1)
34 Five Fields Road
Madison, CT 06443
Attn: Mr. Thomas Reddy

Jet Propulsion Laboratory (1)
4800 Oak Grove Drive
Pasadena, CA 91103
Attn: Mr. Harvey Frank
Mail Stop 198-220

Naval Surface Weapons Center (1)
White Oak Laboratory
Code R-33 (M/S A026)
Silver Spring, MD 20910
Attn: Dr. D. Ernst

Energy Conversion Branch Code 3642 (1)
Naval Underwater Systems Center
Newport Laboratory
Newport, RI 02840
Attn: Mr. J. R. Moden

NASA-Lewis Research Center (1)
Mail Stop 6-1
21000 Brookpark Road
Cleveland, OH 44135
Attn: Dr. Stuart Fordyce

Naval Undersea Center (1)
Code 608
San Diego, CA 92132
Attn: Mr. Joe McCartney

Altus Corporation (1)
440 Page Mill Road
Palo Alto, CA 94306
Attn: Douglas Glader

MS 488 (1)
NASA-Langley Research Center
Hampton, VA 23665
Attn: J. Bene

Research & Development Division (1)
The Gates Rubber Company
999 S Broadway
Denver, CO 80217
Attn: Mr. Eddie T. Seo

Mail Stop 8C-62 (1)
Boeing Aerospace Company
P. O. Box 3999
Seattle, WA 98124
Attn: Mr. Sidney Gross

Honeywell Technology Center (1)
10701 Lyndale Avenue, South
Bloomington, MN 55420
Attn: Dr. H. V. Venkatasetty

Jet Propulsion Laboratory (1)
Mail Stop 198-220
4800 Oak Grove Drive
Pasadena, CA 91103
Attn: Mr. Aiji Uchiyama

Naval Surface Weapons Center (1)
White Oak Laboratory, Code R-33
Silver Spring, MD 20910
Attn: Dr. Frank Bis